Nat.Lab. NL-UR 816/98

Date of issue: ASAP

New 1/f noise model in MOS Model 9, level 903

A.J. Scholten and D.B.M. Klaassen

Company restricted
©Philips Electronics 1998

Authors' address data: A.J. Scholten WAG01; scholtn@prle
D.B.M. Klaassen WAG13; klaassen@prle

©Philips Electronics N.V. 1998
All rights are reserved. Reproduction in whole or in part is
prohibited without the written consent of the copyright owner.

NL-UR: 816/98

Title: New 1/f noise model in MOS Model 9, level 903

Author(s): A.J. Scholten and D.B.M. Klaassen

Part of project: Compact modelling

Customer: Philips Semiconductors

Keywords: Mos Model 9; 1/f noise; parameter extraction; level 903

Abstract: The $1/f$ noise model in MOS Model 9, level 902, fails to describe the V_{GS} dependence of the input-referred noise, observed in experiments. A new $1/f$ noise model has been selected, and implemented in MOS Model 9, level 903. In this report, its physical background is explained. Moreover, noise measurements and noise parameter extraction on C075 are described. It is shown that the amount of $1/f$ noise in HCMOS6 and C075 is comparable. The geometrical scaling rules of the noise model have been verified experimentally for both n- and p-channel MOSFETs. Moreover, it is shown that the new model gives an improved description of the noise in both linear and saturation regime. The new model is available in PSTAR 3.7 as MOS Model 9, level 903. It will be available in HSPICE 98.2.1 (August '98), and in SPECTRE 4.4.3 (November '98).

Conclusions: MOS Model 9, level 903, contains a new $1/f$ noise model.

- The model describes the bias dependence of the $1/f$ noise very well.
- The geometrical scaling rules of the model have been verified on C075 silicon.
- The following set of parameters is recommended for C075:

		N-channels	P-channels
NFMOD=1	N_{FAR} ($\mathrm{V^{-1}m^{-4}}$)	39.8×10^{23}	15.4×10^{23}
	N_{FBR} ($\mathrm{V^{-1}m^{-2}}$)	3.24×10^{8}	0.179×10^{8}
	N_{FCR} ($\mathrm{V^{-1}}$)	0	0.148×10^{-7}
NFMOD=0	N_{FR} ($\mathrm{V^{2}}$)	19.91×10^{-11}	5.81×10^{-11}

©Philips Electronics N.V. 1998

©Philips Electronics N.V. 1998

Contents

1 Introduction **1**

2 Low-frequency noise in MOSFETS **3**
2.1 Low-frequency noise spectrum of a MOSFET 3
2.2 Output noise current and input-referred noise voltage sources 4
2.3 The $1/f$ noise model in MOS Model 902 and its limitations 5

3 New $1/f$ noise model **9**
3.1 Qualitative description 9
3.2 MOS Model 9, level 903 $1/f$ noise model 10
3.3 Relation with the BSIM3v3 model 12

4 Noise measurements on C075 **13**
4.1 Test structures 13
4.2 DC-characterization 14
4.3 Experimental setup and data handling 16
4.4 Sample-to-sample spread and comparison with HCMOS6 18
4.5 Verification of the geometrical scaling rules 20
4.6 Parameter extraction 22
4.7 Improved modelling accuracy in the linear regime 23

5 Conclusion **25**

A Noise in MOSFETs: theory **27**
A.1 General method for noise calculations in MOSFETs 27
A.2 Application of Hooge's law to a MOSFET 29

B The level 903 $1/f$ noise model **31**
B.1 Derivation of the model by Hung *et al.* 31
B.2 Rewriting Hung's model in MOS Model 9 terms 33
B.3 The transition between weak and strong inversion 36
B.4 The value of N^* 37
B.5 Scaling rules 37
B.6 Simplified model and physical interpretation of the parameters 38
B.7 Hooge's law 39

C List of used symbols **41**

References **45**

Distribution

 ©Philips Electronics N.V. 1998

1 Introduction

The modelling of low-frequency noise, and $1/f$ noise in particular, is becoming increasingly important. Evidently, $1/f$ noise limits the performance of low-frequency circuits. Moreover, in high-frequency and RF applications, such as phase-locked loops and voltage-controlled oscillators, $1/f$ noise plays an important role as well. In the case of an oscillator, for instance, the low-frequency noise may mix with the oscillation frequency, resulting in an unwanted increase of the signal bandwidth.

The $1/f$ noise model in MOS Model 9, level 902 [1, 2, 3], is a simple, empirical model. It assumes the input-referred noise (see Sec. 2.2) to be independent of bias conditions. It has been observed in experiments, however, that this is not true (see Fig. 1 and Ref. [4]). In saturation, the input-referred noise is seen to increase with $V_{\rm GS}$, in particular for p-channel devices (Fig. 1). In practice, the $1/f$ noise parameter $N_{\rm FR}$ is tuned in such a way that the measurements for $V_{\rm GS}$ somewhat above $V_{\rm TO}$ are modelled accurately. The reason for this is that this is the most important bias condition in circuit design.

Because of the limitations of the level 902 $1/f$ noise model, alternative models have been studied. A new model has been selected which has the advantages that it is based on physics and that it describes the $1/f$ noise accurately in all operating regimes of the MOSFET. Fig. 1 clearly shows the improvement for a series of p-channel MOSFETs in the saturation regime. This new model is now available as MOS Model 9, level 903 in PSTAR 3.7. It will be implemented in the August '98 release of HSPICE (HSPICE 98.2.1), and in SPECTRE 4.4.3 (november '98).

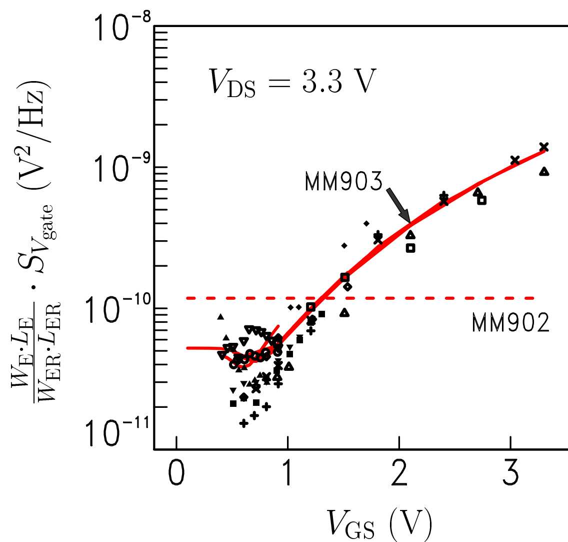

Figure 1: The input-referred noise, multiplied by $W_{\rm E}L_{\rm E}/W_{\rm ER}L_{\rm ER}$, as a function of gate voltage for a number of C075 p-channel MOSFETs in saturation. The dashed line represents the level 902 $1/f$ noise model, the solid lines represent the new $1/f$ noise model available in level 903. See Sec. 4 for more details.

©Philips Electronics N.V. 1998

This report is organized as follows: In chapter 2, we will introduce the reader to the subject of low-frequency noise in MOSFETs. For reasons of tractability, mathematical derivations are postponed to appendix A.
Then, in chapter 3 the physical background of the new $1/f$ noise model will be explained qualitatively. The derivation of the model is elucidated in appendix B.
In chapter 4, the measurements are described that were performed on C075 silicon. In that chapter we will show that the new $1/f$ noise model is capable of describing the measurement results accurately in all operating regimes of the MOSFET. Moreover, the geometrical scaling rules are verified on a set of 11 geometries. The extraction of the noise parameters is discussed.
Finally, in chapter 5, this work is summarized and the conclusions are presented. A list of all the symbols, used throughout this report, is given in appendix C.

 ©Philips Electronics N.V. 1998

2 Low-frequency noise in MOSFETS

2.1 Low-frequency noise spectrum of a MOSFET

Generally, the low-frequency noise spectrum of a MOSFET contains two contributions, see Fig. 2. One contribution is 'white', i.e. independent of the frequency f. This is the so-called 'thermal noise'. The thermal noise model in MOS Model 9 will be discussed in a separate report [5]. The other contribution to the noise spectrum has a frequency dependence which is (approximately) inversely proportional to the frequency f, and is therefore known as '$1/f$ noise'.
Occasionally, MOS transistors exhibit also generation-recombination noise, giving a so-called Lorentzian contribution in the noise spectrum [7, 8]:

$$S_I \propto \frac{\tau}{1 + 4\pi^2 f^2 \tau^2} \tag{1}$$

where τ is the time constant[1] of the traps. Generally, this type of noise is absent for industrial CMOS processes.
For submicrometer-size MOSFETs, 'random telegraph signals' may be observed as well. These are discrete modulations of the channel current due to the capture and emission of channel carriers by a single trap, located near the channel. The electrostatic field of this trap fluctuates and modulates the surface potential in the channel, which, in turn, causes the current to fluctuate. In the frequency domain, this type of noise has the same shape as generation-recombination noise, i.e. a Lorentzian spectrum.
In most cases, however, only thermal and $1/f$ noise is observed.

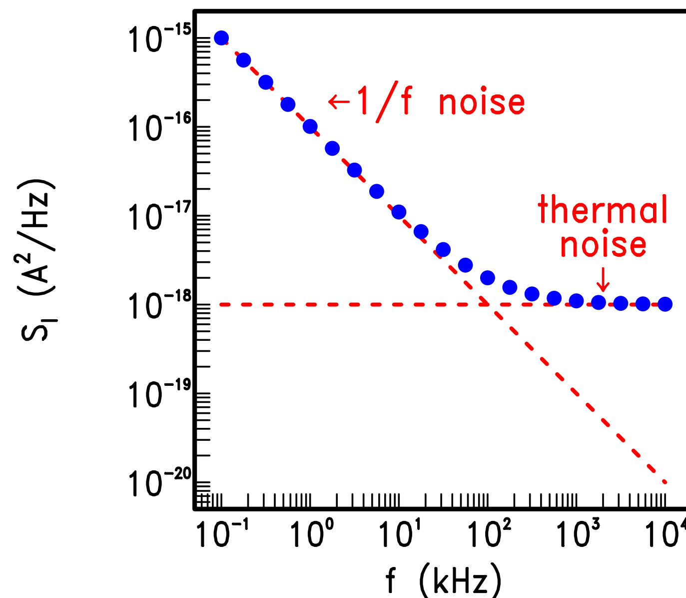

Figure 2: Example of a low-frequency noise spectrum of a MOSFET. The thermal noise and $1/f$ noise contributions are indicated.

[1] More precisely: τ is given by $\frac{1}{\tau} = \left(\frac{d\mathcal{R}}{d\mathcal{N}} - \frac{d\mathcal{G}}{d\mathcal{N}}\right)\Big|_{\mathcal{N}_0}$ where $\mathcal{G}$ and $\mathcal{R}$ are the generation and recombination rates, respectively. See Ref.[7]

©Philips Electronics N.V. 1998

2.2 Output noise current and input-referred noise voltage sources

A MOS transistor that exhibits $1/f$ noise can be represented by adding a noise source to a noiseless MOSFET. This can be done in two different ways, as illustrated in Fig. 3. The first way is adding a $1/f$ *current* noise source in parallel to the transistor. The second way is putting a $1/f$ *voltage* noise source in the lead connecting the gate.

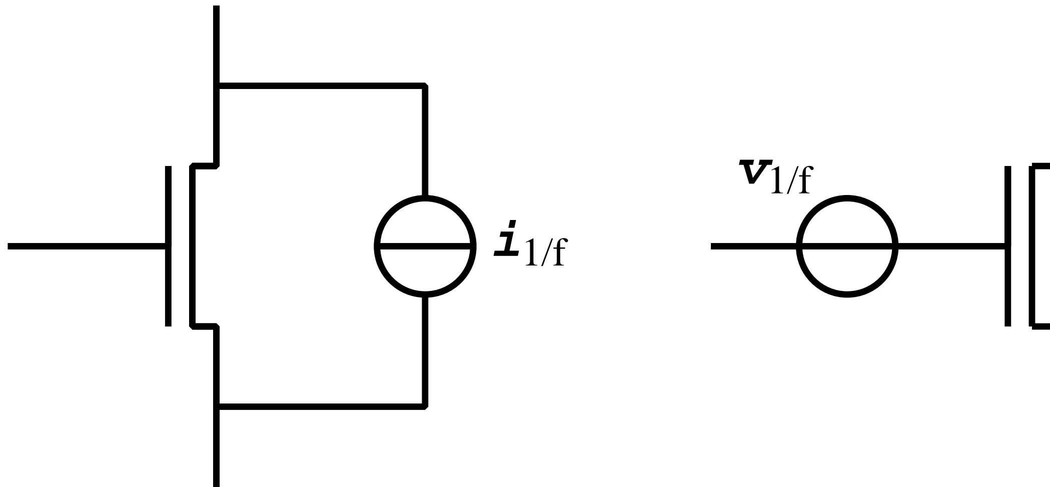

Figure 3: *Left:* $1/f$ output current noise source of a MOS transistor.
Right: input referred $1/f$ voltage noise source.

The input referred noise voltage spectral density $S_{V_{\rm gate}}$ follows from the output noise current spectral density S_I by:

$$S_{V_{\rm gate}} = \frac{S_I}{g_{\rm m}^2}\ , \tag{2}$$

where $g_{\rm m} \equiv \frac{\partial I_{\rm DS}}{\partial V_{\rm GS}}$ is the transconductance.
Both ways of describing the noise are used in practice and are equally valid. At first sight, a description in terms of S_I seems more natural because both the thermal and $1/f$ noise originate from the conducting channel. In this report however, we will focus on $S_{V_{\rm gate}}$ for the following reasons:

1. Just like the drain current itself, the quantity S_I varies over many orders of magnitude, when the bias voltages are varied. The quantity $S_{V_{\rm gate}}$, on the other hand, only varies over 1 or 2 orders of magnitude, making it much easier to observe differences between model and measurements in a graph.

2. According to the 'old' 1/f noise model (i.e. MOS Model 9, level 902), $S_{V_{\rm gate}}$ is, for a given frequency, independent of V_{DS} and V_{GS}, as we will see in section 2.3. Thus in graphs of $S_{V_{\rm gate}}$ the old $1/f$ noise model is constant. Thus plotting

 ©Philips Electronics N.V. 1998

$S_{V_{\rm gate}}$ makes the shortcomings of the old $1/f$ noise model and differences with the new model clearly visible.

3. In circuit analysis, the quantity $S_{V_{\rm gate}}$ is more relevant than S_I. This is because the noise figure F, i.e. the ratio of signal-to-noise power ratios at the input and the output of the device, is directly related to $S_{V_{\rm gate}}$ by [4, 6]

$$F = 1 + \frac{S_{V_{\rm gate}}}{S_{V,{\rm input}}} \tag{3}$$

2.3 The $1/f$ noise model in MOS Model 902 and its limitations

A large variety of explanations for $1/f$ noise is found in the literature, which can be divided in two major categories. One is the McWorther trapping theory, the other the mobility fluctuation theory of Hooge. The noise model presented in this report, in fact, is a combination of these two models.
A simple, but already very useful formula for $1/f$ noise in a MOSFET is obtained if one assumes the empirical "Hooge's law" to be valid microscopically. This leads to

$$S_I = \alpha_{\rm H} \cdot \frac{q\mu_{\rm eff} I_{\rm DS} V_{\rm DS}}{fL^2} \tag{4}$$

The derivation of this formula is found in Sec. A.2. The major drawback of this formula for compact modelling is that it underestimates the measurements considerably near $V_{\rm TO}$, which is the most important bias condition for circuit simulation. Therefore, MOS Model 9, level 902, contains another noise model, which is purely empirical. The MM902 expression for $S_{\rm fl}$, the flicker noise contribution in the noise current spectral density, reads:

$$S_{\rm fl} = N_{\rm F} \cdot \frac{g_{\rm m}^2}{f} \tag{5}$$

Here, $S_{\rm fl}$ is the flicker noise contribution in the noise current spectral density. In terms of input referred noise the above equation simplifies to:

$$S_{V_{\rm gate}} = \frac{N_{\rm F}}{f} \tag{6}$$

The geometrical scaling rule for $N_{\rm F}$ reads:

$$N_{\rm F} = N_{\rm FR} \cdot \frac{W_{\rm ER} L_{\rm ER}}{W_{\rm E} L_{\rm E}} \tag{7}$$

Note that there is no explicit temperature scaling rule. There is only an implicit temperature dependence of the output current noise via $g_{\rm m}$.
Measurements have shown that there are some limitations to this model [4]. In saturation, the input-referred noise is seen to increase with $V_{\rm GS}$, in particular for p-channel devices (Fig. 4). In practice, the parameter $N_{\rm F}$ is tuned in such a way

©Philips Electronics N.V. 1998

that the measurements for V_{GS} somewhat above V_{TO} are modelled accurately (see Fig. 4)., the reason being that this is the most important bias condition in circuit design.
Because of the limitations of the level 902 $1/f$ noise model, described above, alternative $1/f$ noise models have been studied. A new $1/f$ noise model has been selected and incorporated in MOS Model 9. This new model is available in MOS Model 9 level 903. It can be selected by setting the switch NFMOD to 1. By default, this switch is set to 0, which selects the level 902 $1/f$ noise model. This construction makes the level 903 model backwards compatible, i.e. old parameter sets can still be used in level 903, yielding the same results as before.
MOS Model 9, level 903, is already available in PSTAR 3.7, and it will be implemented in HSPICE 98.2.1 (August '98), and in SPECTRE 4.4.3 (November '98).

 ©Philips Electronics N.V. 1998

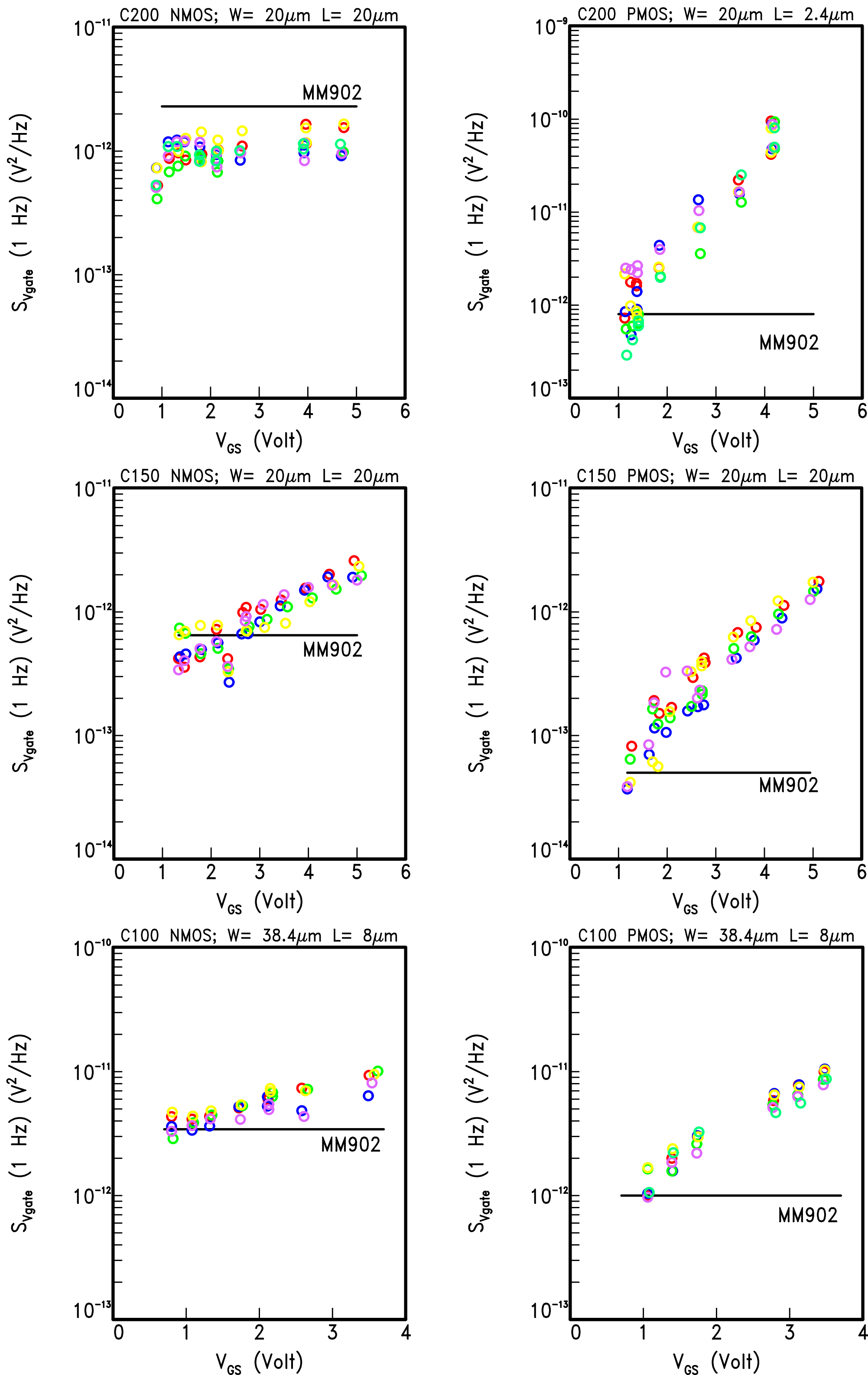

Figure 4: Measurements (from Ref. [4]) of the input-referred $1/f$ noise as a function of gate voltage for MOSFETs in saturation, for the C200, C150 and C100 processes. Different grey scales correspond to different, nominally identical, devices. Solid lines represent the MM902 model, using $N_{\rm FR}$ from the design manuals. *Left:* n-channels. *Right:* p-channels.

©Philips Electronics N.V. 1998

 ©Philips Electronics N.V. 1998

3 New $1/f$ noise model

3.1 Qualitative description

The new $1/f$ noise model is based on two papers by K.K. Hung *et al.* [9, 10]. It assumes trapping and detrapping of charge carriers in the gate oxide to be responsible for the observed $1/f$ noise. This is illustrated in Fig. 5.

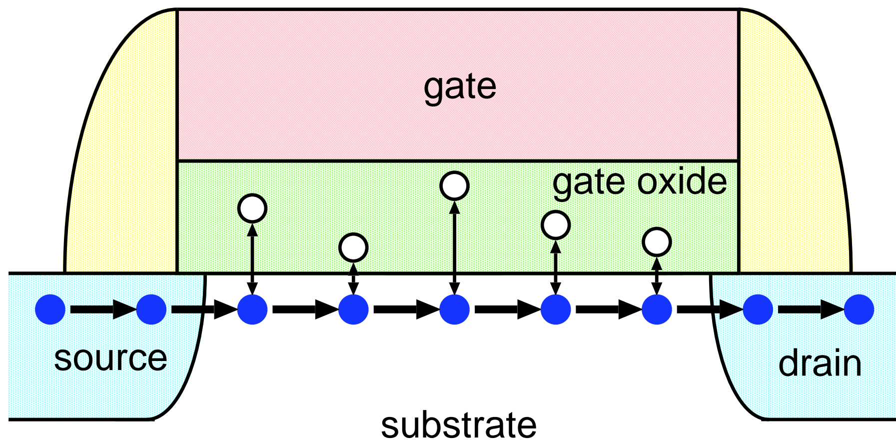

Figure 5: Physical background of the new $1/f$ noise model.

The trapping and detrapping processes causes the number of carriers to fluctuate, which of course leads to fluctuations in the current. Moreover, the trapping of a charge carrier leads to a change of the electric field experienced by the charge carriers in the inversion layer. In other words, not only the number of carriers, but also the mobility fluctuates. Evidently, the two effects are correlated, which is taken into account in the model.

The most characteristic feature of $1/f$ noise is, of course, its spectrum. How is this spectrum explained in the new model? Let us first assume that we have a single trap in the oxide, characterized by a single time constant τ. In this case "random telegraph signals" (RTS), may be observed in the time domain, i.e. the measured current switches back and forth between two (or more) discrete levels. In the frequency domain, this leads to a Lorentzian noise spectrum:

$$\frac{\tau}{1 + 4\pi^2 f^2 \tau^2} \tag{8}$$

The type of fluctuations described here are indeed sometimes observed for very-small sized MOSFETs, where a single, strategically located trap may dominate the fluctuations.

For larger MOSFETs, however, there is usually more than one trap and thus a *distribution* of trapping sites in the oxide. This leads to a distribution of trapping

©Philips Electronics N.V. 1998

times

$$\tau = \tau_0(E) \cdot \exp(\gamma_{\text{ox}} \cdot z) \tag{9}$$

where z is the distance between traps and interface, $\gamma_{\text{ox}} \approx 1$ Å^{-1} is the attenuation coefficient of the electron wave function in the gate oxide, and $\tau_0(E)$ is the time constant of traps located at the Si/SiO$_2$ interface ($z = 0$). It is the integration over z that leads to a $1/f$ spectrum, if the trap distribution is spatially uniform, in particular near the interface. This is illustrated in Fig. 6. Deviations from 'true' $1/f$ noise, e.g. $1/f^\gamma$ noise, can be understood in terms of deviations from a spatially uniform distribution of traps. However, no systematic trends of this exponent γ are known as a function of bias conditions or geometry. Therefore, it makes no sense to take these deviations from 'true' $1/f$ noise into account in compact modelling.

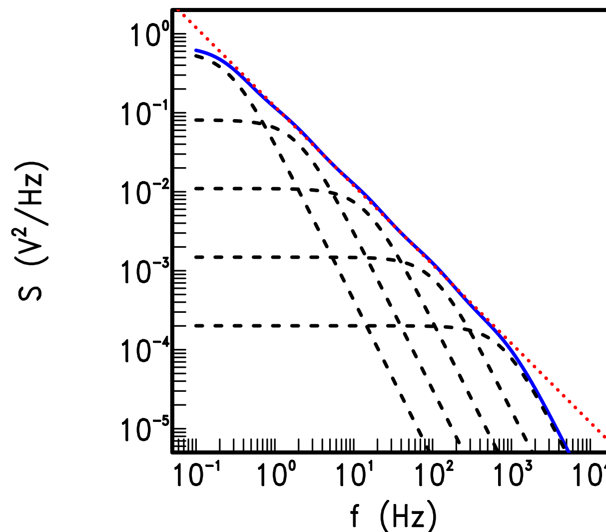

Figure 6: The addition of only 5 Lorentzians (dashed lines) already leads to a $1/f$-like spectrum (solid line) over a considerable frequency range. For reference, the dotted line represents true $1/f$ noise.

The theory, described qualitatively here, is worked out in detail in Refs. [9, 10], and elucidated in appendix B, and leads to the model formulation presented in the next section.

3.2 MOS Model 9, level 903 $1/f$ noise model

The new $1/f$ noise model in MOS Model 9, level 903, can be selected by setting the switch NFMOD to 1. Then, in strong inversion, the $1/f$ noise spectral density is given by Eq. (73) in Appendix B (for the meaning of the used symbols, the reader is referred to appendix C):

 ©Philips Electronics N.V. 1998

$$S_{\rm si} = \frac{\phi_{\rm T}\, q^2 I_{\rm DS}\, \beta\, t_{\rm ox}^2}{f \epsilon_{\rm ox}^2 \left\{1 + \theta_1 V_{\rm GT1} + \theta_2 \cdot (u_{\rm s} - u_{\rm s0})\right\}} \times \left[N_{\rm FA} \cdot \ln \frac{N_0 + N^*}{N_{\rm L} + N^*} + N_{\rm FB} \cdot (N_0 - N_{\rm L}) + \frac{1}{2} \cdot N_{\rm FC} \cdot (N_0^2 - N_{\rm L}^2)\right] + \frac{\phi_{\rm T}\, I_{\rm DS}^2}{f} \cdot \frac{G_2 - 1}{G_2} \cdot \left[\frac{N_{\rm FA} + N_{\rm FB} N_{\rm L} + N_{\rm FC} N_{\rm L}^2}{(N_{\rm L} + N^*)^2}\right] \tag{10}$$

Here we have introduced three miniset parameters $N_{\rm FA}$, $N_{\rm FB}$, $N_{\rm FC}$. Note that the last term, containing G_2 which describes channel-length modulation, is the contribution of the pinch-off region to the $1/f$ noise. In the above formula, we have introduced N_0 and $N_{\rm L}$, which are the (approximate) expressions for the inversion charge densities at the source and drain sides of the channel, respectively:

$$N_0 = \frac{\epsilon_{\rm ox}}{q t_{\rm ox}} \cdot V_{\rm GT3} \tag{11}$$

$$N_{\rm L} = \frac{\epsilon_{\rm ox}}{q t_{\rm ox}} \cdot (V_{\rm GT3} - V_{\rm DS1}) \tag{12}$$

Moreover we use the abbreviation N^*:

$$N^* = \frac{\epsilon_{\rm ox}}{q t_{\rm ox}} \cdot \phi_{\rm T} \cdot (m_0 + 1) \tag{13}$$

The weak inversion expression for the $1/f$ noise spectral density reads:

$$S_{\rm wi} = N_{\rm FA} \cdot \frac{\phi_{\rm T} I_{\rm DS}^2}{f {N^*}^2} \tag{14}$$

The weak and strong inversion expressions are linked as follows: for a given bias point both $S_{\rm wi}$ and $S_{\rm si}$ are calculated. Now the flicker noise at this bias point is given by:

$$S_{\rm fl} = \frac{S_{\rm si} \times S_{\rm wi}}{S_{\rm si} + S_{\rm wi}} \tag{15}$$

This guarantees a smooth transition of the 1/f noise, going from weak to strong inversion. Note that this transition has the consequence that the parameter $N_{\rm FA}$ has to be non-zero: if $N_{\rm FA} = 0$, then $S_{\rm fl} = 0$, irrespective of the values of $N_{\rm FB}$, $N_{\rm FC}$, and bias conditions.

The geometrical scaling of the model is identical to that of MOS MODEL 9, level 902, (and many other models):

$$\left.\begin{array}{rcl} N_{\rm FA} & = & \frac{W_{\rm ER} L_{\rm ER}}{W_{\rm E} L_{\rm E}} \cdot N_{\rm FAR} \\ N_{\rm FB} & = & \frac{W_{\rm ER} L_{\rm ER}}{W_{\rm E} L_{\rm E}} \cdot N_{\rm FBR} \\ N_{\rm FC} & = & \frac{W_{\rm ER} L_{\rm ER}}{W_{\rm E} L_{\rm E}} \cdot N_{\rm FCR} \end{array}\right\} \quad S_{V_{\rm gate}} \propto \frac{1}{W_{\rm E} L_{\rm E}} \text{ (approximately)} \tag{16}$$

The temperature dependence, on the other hand, is changed ($\phi_{\rm T}$ is in the equations), but there are *no* explicit temperature scaling rules of the parameters. The implicit temperature scaling is approximately:

$$S_{V_{\rm gate}} \propto T \tag{17}$$

3.3 Relation with the BSIM3v3 model

The noise model presented above is also used in BSIM3v3 [11]. The parameters used in BSIM3v3 are "Noia", "Noib", and "Noic". They can be calculated from our parameters by:

$$\text{Noia} = 0.01 \cdot \gamma_{\text{ox}} W_{\text{ER}} L_{\text{ER}} \cdot N_{\text{FAR}} \quad [\text{in V}^{-1}\text{m}^{-3}] \tag{18}$$

$$\text{Noib} = 0.01 \cdot \gamma_{\text{ox}} W_{\text{ER}} L_{\text{ER}} \cdot N_{\text{FBR}} \quad [\text{in V}^{-1}\text{m}^{-1}] \tag{19}$$

$$\text{Noic} = 0.01 \cdot \gamma_{\text{ox}} W_{\text{ER}} L_{\text{ER}} \cdot N_{\text{FCR}} \quad [\text{in V}^{-1}\text{m}] \tag{20}$$

Our parameters differ from the BSIM3v3 parameters because

- in contrast to BSIM3v3, we have formulated the model in miniset-maxiset terms;
- the parameters need to be of the order of magnitude that can be handled by PSTAR. This is the reason that γ_{ox} is absorbed in our parameters.

Note that the BSIM3v3 manual erroneously states that "Noia", "Noib", and "Noic" have no unit [11]. Typical magnitudes for the BSIM3v3 noise parameters are Noia $\sim 10^{20}\text{V}^{-1}\text{m}^{-3}$, Noib $\sim 10^{4}\text{V}^{-1}\text{m}^{-1}$, and Noic $\sim 10^{-12}\text{V}^{-1}\text{m}$.
It should be noted that there are two differences between our $1/f$ noise model and the BSIM3v3 $1/f$ noise model:

1. The transition between weak and strong inversion has been smoothed in our implementation, See Eq. (15). This is discussed in Appendix B.3 and in Ref. [12].
2. We use the physically correct value of N^*, i.e. Eq. (13). In BSIM3v3 N^* has been fixed to an arbitrary value of 2×10^{14} m^{-2}. We found, however, that using Eq. (13) gives better modelling results. For more details see Sec. B.4 or Ref. [13].

 ©Philips Electronics N.V. 1998

4 Noise measurements on C075

4.1 Test structures

A number of test structures has been processed on the C075 multiproject wafer M4YN491X1. The geometries are listed in table 1. Apart from some "conventional" device sizes[2] like 10/5 and 5/10, a number of wide, short devices was chosen, like 2000/1 and 400/0.35. The reason for this, is that it is these devices that determine the $1/f$ noise in practical circuits. Moreover these devices have a large g_{m}, which allows us to perform measurements in the subthreshold regime, which is not feasible for "conventional" device geometries.

$\downarrow L\ \ W \rightarrow$	2000	400	200	100	50	10	5
10							X
5		X			X	X	
1	X	X	X	X	X		
0.35		X	X				

Table 1: Geometries used for the noise measurements. W and L are in μm.

In the design of these structures, the following issues are of interest:

1. **No gate protection.** The use of a gate protection may have influence on the amount of $1/f$ noise. In a practical circuit, a gate protection is not present for the MOSFET that determines the noise. Therefore, we did not use a gate protection for our test structures as well. As a consequence, we used separate gate connections for all devices in one module, so that the possible breakdown of one device does not affect the others.

2. **Avoiding M1.** The M1 level in C075 is tungsten, which has a much higher specific resistance than aluminum, which is the metal used in M2-M5. Therefore, the connection of drain and source was done in M2. The connection of gate was made in M5. M1 was only used for an extra connection 'rails' to connect the bulk.

3. **Folding.** Wide transistors were always folded in such a way that the resulting area resembles a square as much as possible. Moreover, the folding factor was always even, which leads to smaller drain capacitances. This is in accordance with the way that these transistors are layed out in practice. Note: due to this folding, some transistors can have a minor deviation in width, compared to the values listed in table 1.

All measurements were performed on packaged devices, because no experimental setup for on-wafer noise measurements was available at the time of the measurements.

[2]We use the notation 10/5 to indicate $W = 10$ μm and $L = 5$ μm.

©Philips Electronics N.V. 1998

4.2 DC-characterization

Standard MOS Model 9 characterization was performed on the multiproject wafer. A HP 4155B analyzer was used for these DC-measurements. The analyzer was controlled by the HP IC-CAP5.0 program, using a LAN interface (HP E2050 Gateway) to connect the HPIB-bus of the analyzer to the Local Area Network (LAN), see Fig. 7.

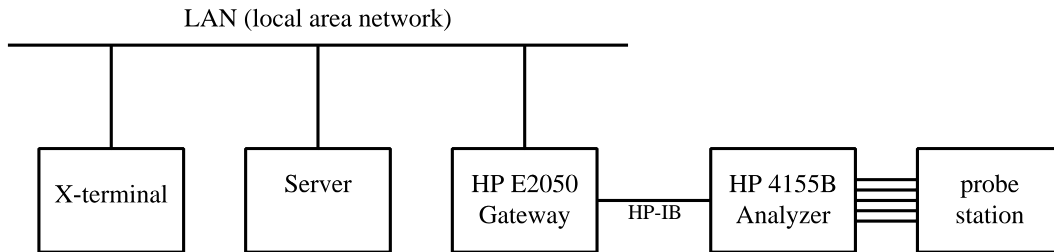

Figure 7: Schematic overview of the DC measurement setup

A MOS Model 9 simulation, using the C075FM 2.01 parameter set, was performed. Both for n- and p-channels it was found that this parameter set gives a satisfactory description of both the linear and saturation regime. This indicates that the silicon used is on target.
The subthreshold modelling, however, was not sufficiently accurate to model g_{m} accurately in this regime. (As we will see in Sec. 4.3, we need this g_{m} to calculate the input-referred noise voltage.) To improve the modelling accuracy, we adjusted the threshold voltage parameters, leaving the other parameters unchanged. The threshold voltage parameters were adjusted as shown in Table 2. The change of parameters corresponds to a threshold voltage shift which is nearly independent of channel length and amounts to $\sim$ 100 mV and $\sim$ 10 mV for n- and p-channels, respectively. The width dependence of V_{TO}, as expressed by the parameter $S_{W;V_{\mathrm{TO}}}$, seems to have changed considerably. Note however that in the width range of our samples (5 – 2000 μm), the value $S_{W;V_{\mathrm{TO}}} = 100\times10^{-9}$ Vm corresponds to a threshold voltage shift of only 20 mV.

	N-channels		P-channels	
	C075FM 2.01	adjustment	C075FM 2.01	adjustment
V_{TOR} (V)	0.625	0.520	0.595	0.5844
$S_{L;V_{\mathrm{TO}}}$ (Vm)	76.00 $\times10^{-9}$	68.74 $\times10^{-9}$	31.00 $\times10^{-9}$	45.16 $\times10^{-9}$
$S_{L2;V_{\mathrm{TO}}}$ (Vm^2)	-24.80 $\times10^{-15}$	-31.26 $\times10^{-15}$	-11.50 $\times10^{-15}$	-16.25 $\times10^{-15}$
$S_{W;V_{\mathrm{TO}}}$ (Vm)	3.490 $\times10^{-9}$	108.5 $\times10^{-9}$	-11.20 $\times10^{-9}$	81.48 $\times10^{-9}$

Table 2: Adjustment threshold voltage parameters with respect to the C075FM 2.01 parameter set

 ©Philips Electronics N.V. 1998

After the adjustment of these parameters, the modelling of in all operating regimes of the MOSFET, and for all geometries, is satisfactory. To illustrate this, we show a comparison of data and model for the 400/0.35 p-channel MOST, see Fig. 8. In these plots, $V_{\rm GS}$ is varied in the saturation region ($V_{\rm DS} = 3.3$ V). This is exactly the bias conditions that are used mostly in the noise measurements.

Note that this procedure (i.e. the use of the C075FM 2.01 parameter set) has been followed in order to obtain noise parameters which can be included in future releases of the MM9 parameter set for C075.

For future noise parameter extraction, we recommend to perform the noise parameter extraction on the same wafer as the DC parameter extraction. (This was not possible now because the DC parameter set has been determined from earlier wafers that did not contain the test structures used in this investigation.)

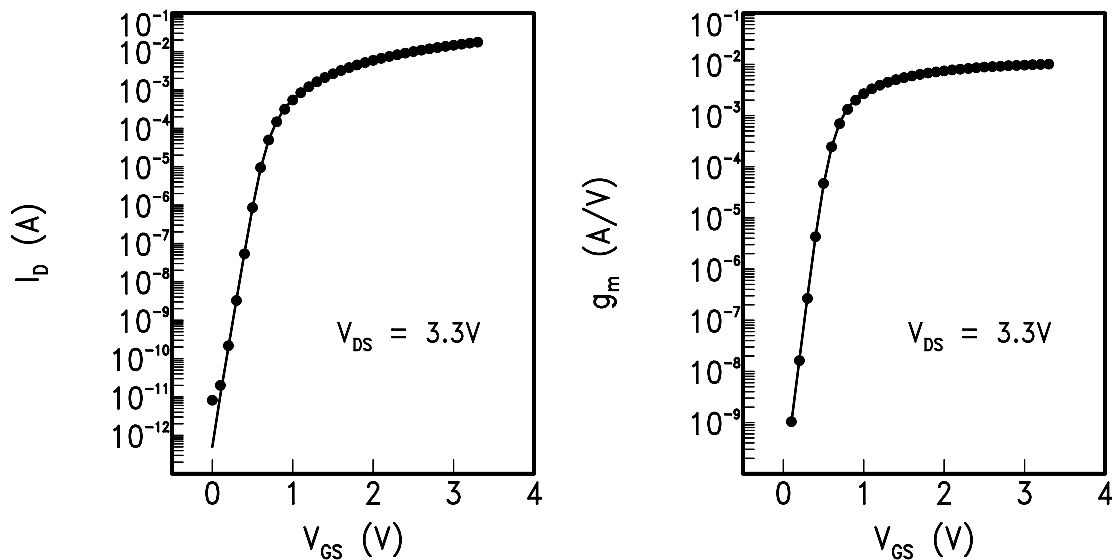

Figure 8: Drain current (*Left*) and transconductance (*Right*) in saturation ($V_{\rm DS} = 3.3$ V) as a function of gate-source voltage for a 400/0.35 p-channel MOST. Symbols are the data, solid line represents MOS Model 9.

4.3 Experimental setup and data handling

The experimental setup, used for the low-frequency noise measurements, is schematically depicted in Fig. 9. The device under study, which is packaged, is mounted in a HP test fixture. The variable voltage sources $V_{\rm GS}$ and $V_{\rm D}$ consist of a battery and a potentiometer. The current fluctuations S_I of the MOSFET are transformed into voltage fluctuations $S_V = S_I \cdot R_{\rm meas}^2$ across the measurement resistor $R_{\rm meas} = 1$ kΩ. These voltage fluctuations, in turn, are amplified by an ultra-low noise amplifier, which is also fed by batteries. The entire setup, described so far, is shielded by a metal closet in order to avoid unwanted interference signals (mainly 50 Hz and higher harmonics), that may spoil the noise measurements. The amplified noise signal is now fed into a spectrum analyzer, located outside the metal closet. The spectrum analyzer is controlled by a personal computer running a dedicated Lab-View program. The noise spectrum was measured in the frequency range 1-1000 Hz. Each spectrum was measured 8 times. This was done in order to check the validity of the measurements (no outliers). From these 8 spectra, both the average and the standard deviation associated with each measurement frequency were calculated. Typically, this standard deviation appeared to be $\sim$ 10 % of the measurement value.
Using the experimental setup described above, noise spectra were measured for both p-channel and n-channel devices of different geometries. Most measurements were performed in the saturation regime, where $V_{\rm DS}$ was kept at $\sim$ 3.3 V. For each measurement, it was checked that it exceeds the background noise contributions of low-noise-amplifier and measurement resistor significantly.
The spectra all showed a $1/f$-like behavior. A $1/f$ spectral density was fitted to the noise spectrum. Sometimes a white noise contribution was added to account for background noise contributions. Some typical examples of measurements and curve fits are shown in Fig. 10. The standard deviations, determined as explained in the previous section, were taken into account in the curve fitting.
The result of the $1/f$ curve fit is a voltage noise spectral density at 1 Hz, which applies to the output of the low noise amplifier. From this we calculate the voltage noise at the input of the amplifier by dividing by 1000^2, i.e. the square of the amplifier gain. Subsequently, the current noise spectral density of the MOSFET is found by dividing by $R_{\rm meas}^2$. Finally, as explained in Sec. 2.2, the input-referred voltage noise is obtained by dividing by $g_{\rm m}^2$. The value of $g_{\rm m}$ was obtained from the DC parameter set.

 ©Philips Electronics N.V. 1998

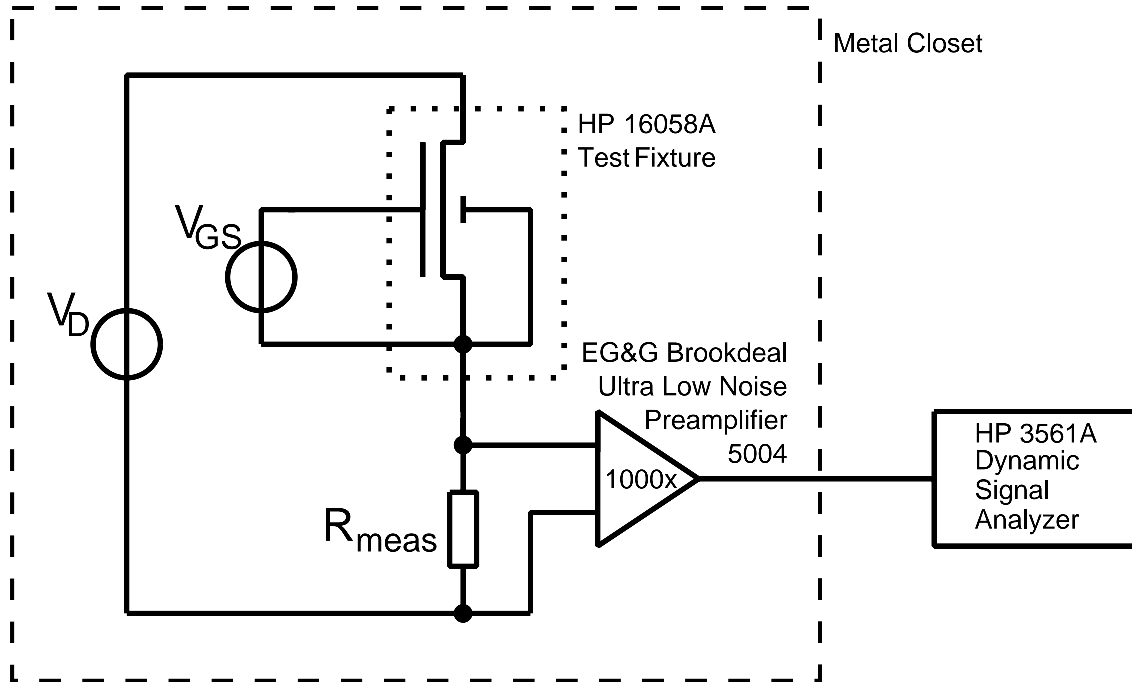

Figure 9: Schematical representation of the experimental setup.

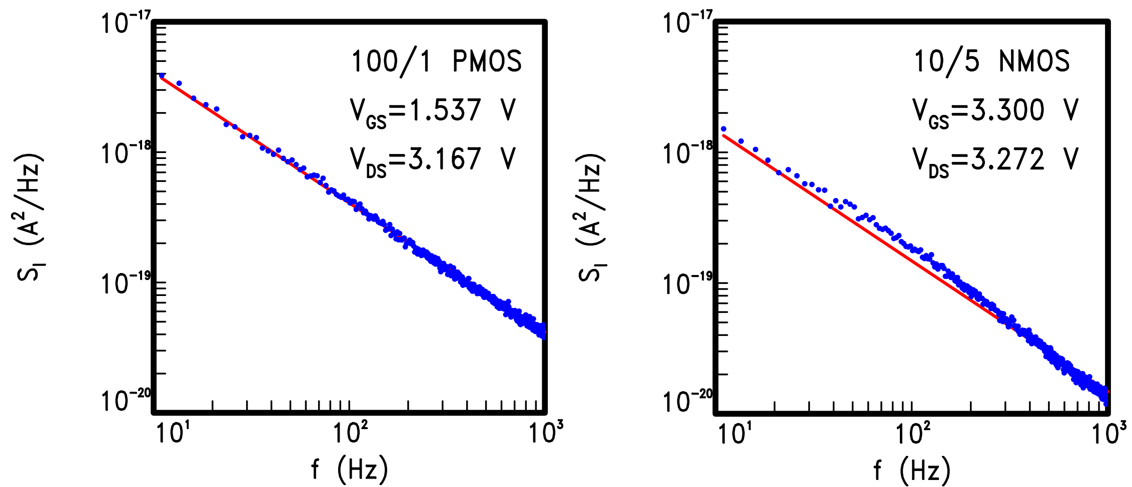

Figure 10: Some typical examples of measured noise spectra. The dots represent the measurements, the solid line the $1/f$ curve fit.

©Philips Electronics N.V. 1998

4.4 Sample-to-sample spread and comparison with HCMOS6

The input-referred $1/f$ noise has been determined as a function of V_{GS} for a number of supposedly identical 10/5 devices. The results, for both n- and p-channels, are shown in Fig. 11. The results for a series of 5/10 samples are shown in Fig. 12. Both the n- and the p-channel curves show an increase of the input-referred noise as a function of V_{GS}, in accordance with earlier results [4]. This increase is much more pronounced for p-channels than for n-channels. For low V_{GS}, the lowest input-referred noise is found for the p-channels, whereas for high V_{GS}, the input-referred noise of n- and p-channels is comparable. Thus the often heard statement that 'p-channels are less noisy than n-channels' only applies to gate-source voltages near V_{TO}.
Another important observation from the measurements is the pronounced sample-to-sample spread, which is comparable to the spread observed by de Boet [4]. It is well-known that this sample-to-sample spread increases considerably for smaller device areas. This is illustrated in Fig. 13, taken from Ref. [4], where the error bars associated with N_{F} are seen to increase considerably for decreasing sample area. For a theoretical description of this sample-to-sample spread the reader is referred to Ref. [14], where the sample-to-sample spread is associated with the stochastic distribution of oxide traps.
Evidently, one has to take this sample-to-sample spread into account during the measurements. Therefore it is recommended for noise measurements:

- always measure a number of devices.
- use sufficiently large devices (area $\gtrsim$ 50 $\mu\mathrm{m}^2$) to reduce sample-to-sample spread.
- use wide and short devices to keep the noise measurable (the measured noise is proportional to W/L^3).

In Fig. 11, a comparison is made between the present data on C075 silicon processed in MOS4, and data on HCMOS6, processed and measured in Crolles. If we assume that the experimental setups in Crolles and Eindhoven are comparable, this leads to the conclusion that the amount of $1/f$ noise in both 0.35 μm processes is also comparable.

 ©Philips Electronics N.V. 1998

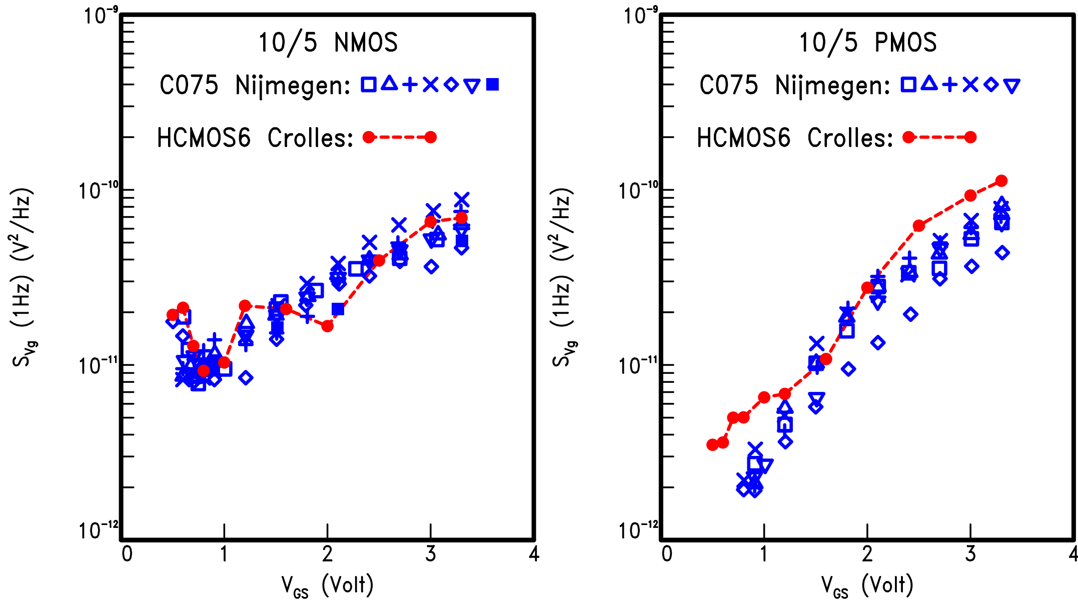

Figure 11: *Left:* Input-referred voltage noise in saturation ($V_{\rm DS}$ = 3.3 V) as a function of gate-source voltage for various, nominally identical, 10/5 n-channel devices processed in C075. The measurements are compared with a measurement from HCMOS6 in Crolles. *Right:* Same, but now for a series of 10/5 p-channel devices.

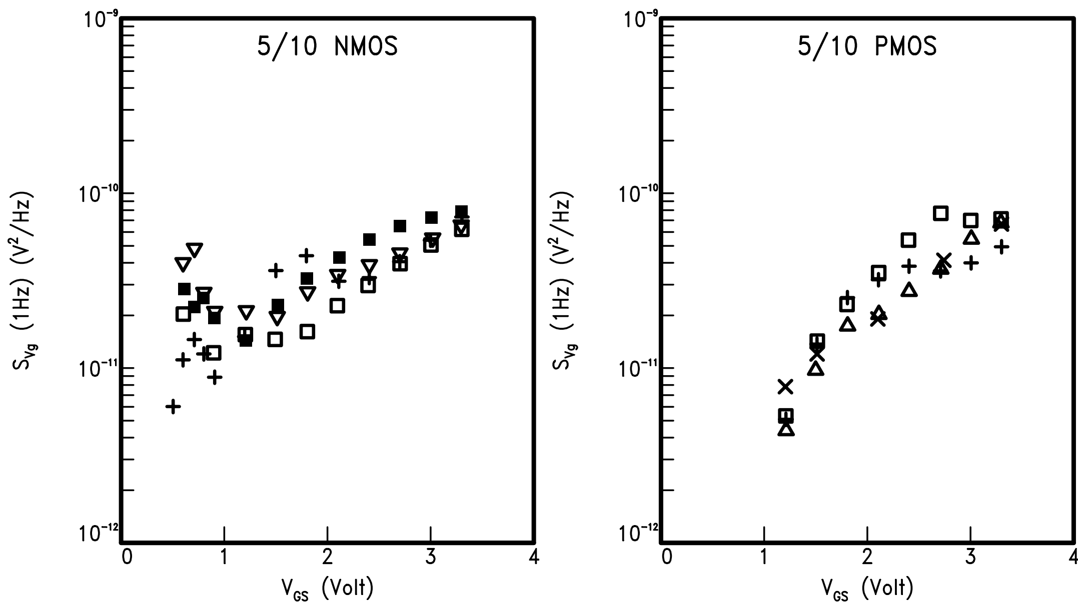

Figure 12: *Left:* Input-referred voltage noise in saturation ($V_{\rm DS}$ = 3.3 V) as a function of gate-source voltage for various, nominally identical, 5/10 n-channel devices processed in C075. *Right:* Same, but now for a series of 5/10 p-channel devices.

©Philips Electronics N.V. 1998

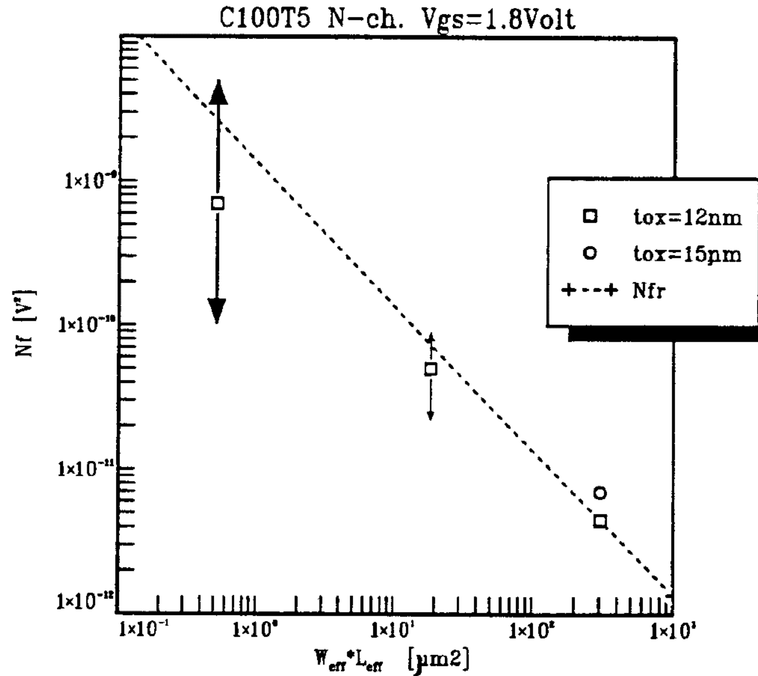

Figure 13: N_{F} as a function of device area for the C100T5 process (Crolles). The inrease of the error bars for smaller device areas is due to the increasing sample-to-sample spread (from Ref. [4]).

4.5 Verification of the geometrical scaling rules

Almost all noise models have a geometrical scaling

$$S_{V_{\mathrm{gate}}} \propto \frac{1}{W_{\mathrm{E}} L_{\mathrm{E}}} \tag{21}$$

The new level 903 $1/f$ noise model is no exception to this. The major geometrical scaling properties of this model are found in the scaling rules for the parameters N_{FA}, N_{FB}, N_{FC}:

$$\begin{aligned} N_{\mathrm{FA}} &= N_{\mathrm{FAR}} \cdot \frac{W_{\mathrm{ER}} L_{\mathrm{ER}}}{W_{\mathrm{E}} L_{\mathrm{E}}} \\ N_{\mathrm{FB}} &= N_{\mathrm{FBR}} \cdot \frac{W_{\mathrm{ER}} L_{\mathrm{ER}}}{W_{\mathrm{E}} L_{\mathrm{E}}} \\ N_{\mathrm{FC}} &= N_{\mathrm{FCR}} \cdot \frac{W_{\mathrm{ER}} L_{\mathrm{ER}}}{W_{\mathrm{E}} L_{\mathrm{E}}} \end{aligned} \tag{22}$$

Apart from this there are some implicit geometrical scaling via second-order effects in I_{DS}, scaling of the θ-parameters, and the term that depends quadratically on I_{DS}. In order to verify this geometrical scaling, we performed noise measurements on a series of 11 different geometries (see Table 1) for both n- and p-channels. For all the

 ©Philips Electronics N.V. 1998

geometries, the input-referred noise voltage was determined as a function of gate-source voltage for $V_{\rm DS} = 3.3$ V. This value was multiplied by the effective device area, and divided by the effective area of the reference device (the 10/0.35 device). The $1/f$ noise of the 10/5 and 5/10 devices could be measured from somewhat above threshold up to the supply voltage. Devices which are wider and shorter, however, have a much larger $g_{\rm m}$, and therefore also a larger DC and $1/f$ noise current. Therefore these devices could be measured also in the subthreshold regime. However, they could not be measured for gate voltages as high as the supply voltage, because the current drive capability of the experimental setup was not large enough to keep the devices in saturation.
The results are shown in Fig. 14. It is observed that all measurements merge nicely onto one curve. No systematic deviations for short-channel devices are observed, and the deviations between different geometries are of the same order of magnitude as the sample-to-sample spread for one geometry (cf. Sec. 4.4). This leads to the conclusion that the geometrical scaling rules of the new $1/f$ noise model are sufficiently accurate.

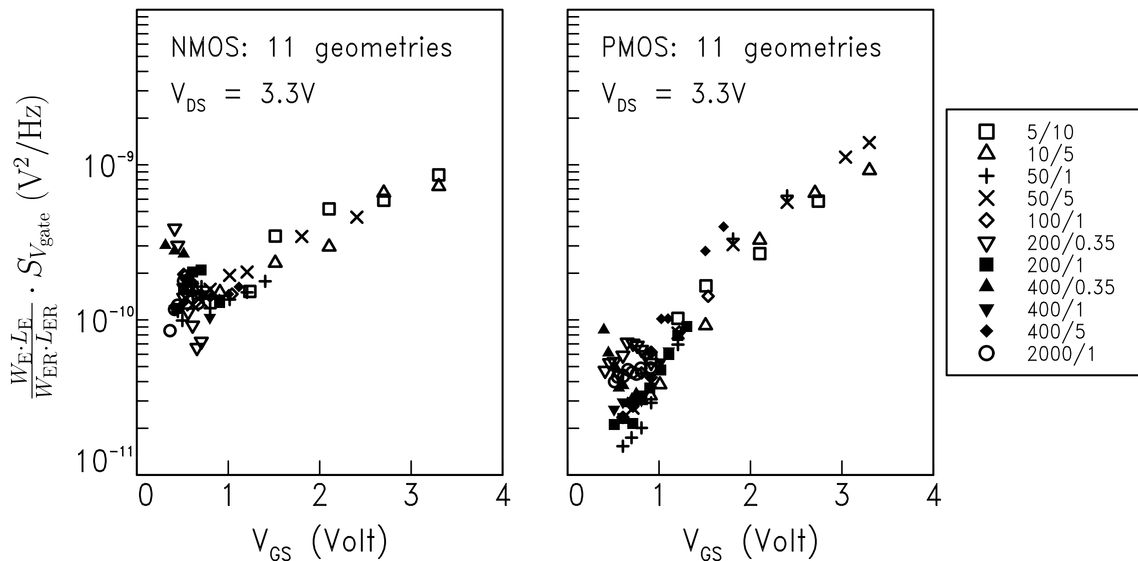

Figure 14: *Left:* Input-referred voltage noise in saturation ($V_{\rm DS} = 3.3$ V), multiplied by the ratio of effective device area and effective reference device area, as a function of gate-source voltage, for a series of n-channel geometries. *Right:* Same, but now for a series of p-channel geometries.

©Philips Electronics N.V. 1998

4.6 Parameter extraction

We have used the following parameter extraction strategy:

- Only data were used with $V_{\mathrm{DS}} > V_{\mathrm{GT}}$ (the saturation region is the most important region for circuit simulation). Included were the measurements of Figs. 11, 12, and 14.
- All these data are used *simultaneously* in fitting N_{FAR}, N_{FBR}, N_{FCR}.
- In compact modelling we rather overestimate the noise than underestimate it. Therefore we forced the fitted curve to the upper side of the measurements. This was achieved in the fitting program, by taking the error, assigned to a situation where the calculated noise exceeds the measured noise, twice the error of the opposite situation.
- For the n-channels, N_{FCR} was not necessary, and set to zero.

The resulting curve fit is shown in Fig. 15 for the series of 11 geometries. For comparison, the level 902 model with the parameters from the 1.03 (A3) process block is shown as well. All the parameters are listed in table 3.

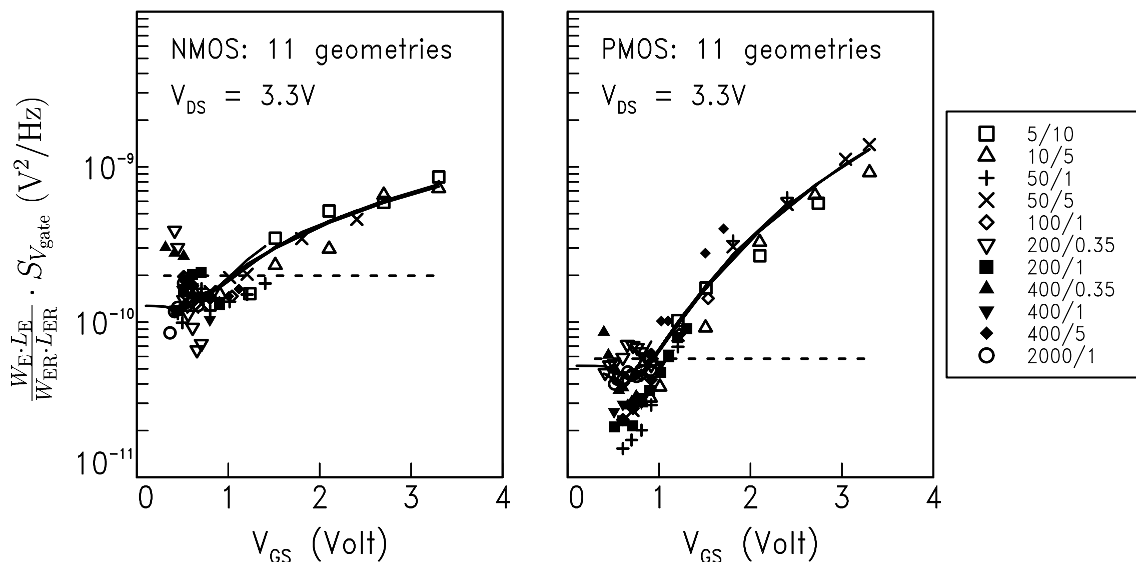

Figure 15: Same as Fig. 14, but now with the new $1/f$ noise model (solid line), and the level 902 $1/f$ noise model (dashed line).

		N-channels	P-channels
NFMOD=1	N_{FAR} ($\mathrm{V}^{-1}\mathrm{m}^{-4}$)	39.8×10^{23}	15.4×10^{23}
	N_{FBR} ($\mathrm{V}^{-1}\mathrm{m}^{-2}$)	3.24×10^{8}	0.179×10^{8}
	N_{FCR} (V^{-1})	0	0.148×10^{-7}
NFMOD=0	N_{FR} (V^{2})	19.91×10^{-11}	5.81×10^{-11}

Table 3: Recommended $1/f$ noise parameters for C075. The parameters N_{FAR}, N_{FBR}, N_{FCR} have been extracted from the present measurements. The parameters N_{FR} for the level 902 model are those found in the 1.03 (or A3) process block.

 ©Philips Electronics N.V. 1998

4.7 Improved modelling accuracy in the linear regime

The parameter extraction, as discussed above, is entirely based on saturation region data, because of the importance of the saturation region in circuit design. It is still interesting, however, to see how well the new model behaves in the linear regime. To investigate this, the 10/5 p-channel device was measured for several gate voltages, and for drain voltages ranging from 0.1 to 3.3 Volt. The result is shown in Fig. 16. The solid lines are calculated using the new model and the parameters extracted in the previous paragraph. The dashed line again represents the level 902 model.
Note that the calculated curves overestimate the noise somewhat throughout the whole bias range. We will explain the reason for this now. The 10/5 p-channel device was one of the devices discussed in the previous section. Thus the data points for $V_{\mathrm{DS}} = 3.3$ V are also found in the right part of Fig. 15 (the triangles $\triangle$). It is seen in that figure that this particular device has a noise level which is somewhat lower than 'average' (i.e. the model curve). Therefore the model curves in Fig. 16, which are based on the same parameters, overestimate the noise as well.
Evidently, the modelling accuracy in the linear regime is enhanced considerably, even though linear region data have not been taken into account in the parameter extraction. Doing so would of course enhance the modelling accuracy even more.

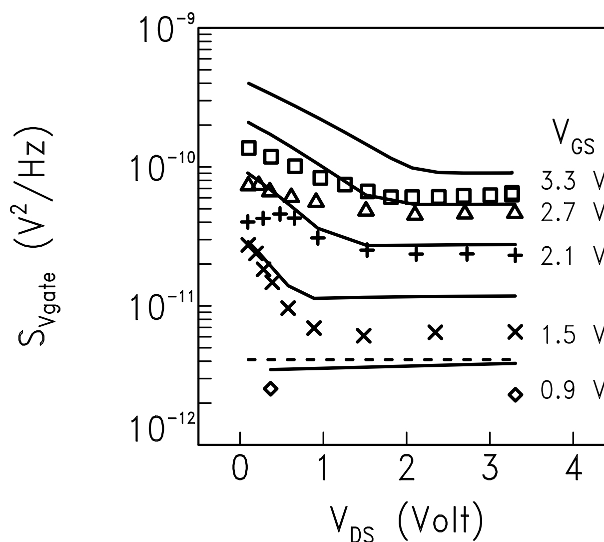

Figure 16: Input-referred $1/f$ noise for a 10/5 p-channel device for a number of bias points in both linear and saturation regime. The solid line represents the new model, evaluated using the parameters extracted in Sec. 4.6. The dashed line corresponds to the MOS Model 902 $1/f$ noise model, using N_{FR} from the 1.03 (or A3) process block.

©Philips Electronics N.V. 1998

©Philips Electronics N.V. 1998

5 Conclusion

MOS Model 9, level 903, contains a new $1/f$ noise model, which accounts for the V_{GS} dependence of the input-referred noise, found in experiments. The model contains three new parameters, N_{FAR}, N_{FBR}, and N_{FCR}, and a switch NFMOD that selects either the old (NFMOD=0) or the new (NFMOD=1) $1/f$ noise model. The physical background of this model has been elucidated in this report.
Noise measurements have been performed on C075 silicon. This led to the following conclusions:

- The present 1/f noise measurements on 0.35 μm silicon from Nijmegen are comparable to the measurements performed in Crolles on HCMOS6. This is an indication that both measurement setups are in order and that the amount of 1/f noise in both processes is comparable.
- The geometrical scaling rules have been verified experimentally, in particular for very wide, short devices that are important in real circuits.
- The new 1/f noise model gives much better results than the level 902 1/f noise model, in *all* operating regimes of the MOSFET.
- The following set of parameters is recommended for C075:

		N-channels	P-channels
NFMOD=1	N_{FAR} ($\mathrm{V}^{-1}\mathrm{m}^{-4}$)	39.8×10^{23}	15.4×10^{23}
	N_{FBR} ($\mathrm{V}^{-1}\mathrm{m}^{-2}$)	3.24×10^{8}	0.179×10^{8}
	N_{FCR} (V^{-1})	0	0.148×10^{-7}
NFMOD=0	N_{FR} (V^{2})	19.91×10^{-11}	5.81×10^{-11}

Acknowledgments

I would like to thank Peter de Vreede for designing the C075 $1/f$ noise test structures, and Heinze Elzinga for putting them on the multiproject wafer. Adrie Zegers is acknowledged for her help in the noise measurements.

©Philips Electronics N.V. 1998

 ©Philips Electronics N.V. 1998

A Noise in MOSFETs: theory

A.1 General method for noise calculations in MOSFETs

First we will address the question how to calculate the current noise $S_I(f)$ on the output terminals of a MOSFET if we know the current noise sources $h(x,t)$ inside the device. We follow Refs. [7, 8, 15]. Note that the derivation is in terms of the quasi-Fermi potential V, which makes the results valid when we have either drift, diffusion or both as transport mechanism. In other words, the result applies to the weak, moderate, and strong inversion regimes of the MOSFET.
The current I_{DS} is given by:

$$I_{\mathrm{DS}} = g(x)\frac{\mathrm{d}V}{\mathrm{d}x} \tag{23}$$

where V is de quasi-Fermi potential of the electrons $g(x)$ is given by

$$g(x) = -W\mu_{\mathrm{eff}}Q_{\mathrm{i}}(x) \tag{24}$$

where $Q_{\mathrm{i}}(x)$ is the inversion charge density in $\mathrm{C/m^2}$.
If we have a current noise source $h(x,t)$ in the channel the current will be $I_{\mathrm{DS}} + \Delta I_{\mathrm{DS}}(t)$ and the quasi-Fermi potential will be $V + \Delta V(t)$. We assume that the source and drain voltages are constant (only I_{DS} fluctuates), so that $\Delta V(t) = 0$ for $x = 0$ and $x = L$. We have

$$I_{\mathrm{DS}} + \Delta I_{\mathrm{DS}}(t) = g(V + \Delta V(t))\frac{\mathrm{d}(V + \Delta V(t))}{\mathrm{d}x} + h(x,t) \tag{25}$$

For small fluctuations this can be written using Taylor expansion as:

$$\begin{aligned} I_{\mathrm{DS}} + \Delta I_{\mathrm{DS}}(t) &\approx \left\{g(V) + \frac{\mathrm{d}g}{\mathrm{d}V}\Delta V(t)\right\}\left\{\frac{\mathrm{d}V}{\mathrm{d}x} + \frac{\mathrm{d}\Delta V(t)}{\mathrm{d}x}\right\} + h(x,t) \\ &\approx g(V)\frac{\mathrm{d}V}{\mathrm{d}x} + g(V)\frac{\mathrm{d}\Delta V(t)}{\mathrm{d}x} + \frac{\mathrm{d}g}{\mathrm{d}V}\frac{\mathrm{d}V}{\mathrm{d}x}\Delta V(t) + h(x,t) \\ &= g(V)\frac{\mathrm{d}V}{\mathrm{d}x} + \frac{\mathrm{d}}{\mathrm{d}x}\left[g(V)\Delta V(t)\right] + h(x,t) \end{aligned} \tag{26}$$

The first term on the right side is equal to I_{DS}, so that the above equation reduces to:

$$\Delta I_{\mathrm{DS}}(t) = \frac{\mathrm{d}}{\mathrm{d}x}\left[g(V)\Delta V(t)\right] + h(x,t) \tag{27}$$

Now we integrate both sides of the equations from $x = 0$ to $x = L$. The first term on the right side now vanishes because of the boundary conditions $\Delta V(t) = 0$ for $x = 0$ and $x = L$. Now we find:

$$\Delta I_{\mathrm{DS}}(t) = \frac{1}{L}\int_0^L h(x,t)\mathrm{d}x \tag{28}$$

Now we have the relation between the current noise sources $h(x,t)$ inside the device and the current fluctuations $\Delta I_{\mathrm{DS}}(t)$ observed in the leads. In order to express this

©Philips Electronics N.V. 1998

relation in terms of noise spectral densities, we first calculate the autocorrelation function of $\Delta I_{\rm DS}(t)$, i.e. the average (over time t) $\overline{\Delta I_{\rm DS}(t)\Delta I_{\rm DS}(t+s)}$,

$$\begin{aligned}\overline{\Delta I_{\rm DS}(t)\Delta I_{\rm DS}(t+s)} &= \overline{\frac{1}{L}\int_0^L h(x,t){\rm d}x\frac{1}{L}\int_0^L h(x',t+s){\rm d}x'} \\ &= \frac{1}{L^2}\int_0^L\int_0^L \overline{h(x,t)h(x',t+s)}{\rm d}x{\rm d}x' \end{aligned} \tag{29}$$

The *Wiener-Khintchine theorem* states that the noise spectral density of a quantity is equal to twice the Fourier transform of the autocorrelation function [7, 8]. Applying this theorem to both sides of Eq. (29), the noise spectral density, $S_I(f)$, is found:

$$S_I(f) = \frac{1}{L^2}\int_0^L\int_0^L S_h(x,x',f){\rm d}x{\rm d}x' \tag{30}$$

where $S_h(x,x',f)$ is the 'spatial cross-spectral intensity' of the noise. Now we assume that we have spatially uncorrelated current noise sources. This means that $S_h(x,x',f)$ can be written as the product of a Dirac δ-function $\delta(x'-x)$ and a function $\mathcal{F}$ that only depends on x' and f:

$$S_h(x,x',f) = \mathcal{F}(x',f)\delta(x'-x) \tag{31}$$

Thus for uncorrelated current noise sources we find:

$$S_I(f) = \frac{1}{L^2}\int_0^L \mathcal{F}(x,f){\rm d}x \tag{32}$$

If we evaluate $S_I(f)$ in a section between x and $(x+\Delta x)$ (we call this quantity $S_{I,\Delta x}(x,f)$), we find:

$$S_{I,\Delta x}(x,f) = \frac{1}{\Delta x^2}\int_0^{\Delta x} \mathcal{F}(x,f){\rm d}x = \frac{\mathcal{F}(x,f)}{\Delta x} \tag{33}$$

Now we know the meaning of $\mathcal{F}(x,f)$:

$$\mathcal{F}(x,f) = S_{I,\Delta x}(x,f)\cdot\Delta x \tag{34}$$

Using this result in Eq. (32) we finally obtain:

$$\boxed{S_I(f) = \frac{1}{L^2}\int_0^L S_{\Delta I}(x,f)\cdot\Delta x\cdot{\rm d}x} \tag{35}$$

Note again that this equation applies to the general case that we have both drift and diffusion. Thus it is equally valid in the subthreshold and strong inversion regimes. The formula (35) is somewhat counterintuitive. In fact, most people starting with noise calculations in MOSFETs would guess:

$$S_V(f) = \int_0^L \frac{S_{V,\Delta x}(x,f)}{\Delta x}{\rm d}x \tag{36}$$

where $S_{V,\Delta x}(x,f)$ is the voltage noise spectral density of a segment Δx. This method of calculating the noise is sometimes referred to as the "Salami method". Generally, it gives wrong results because it assumes the voltage noise spectral densities of two device segments to be uncorrelated. A discussion of this subject is found in Ref.[16].

 ©Philips Electronics N.V. 1998

A.2 Application of Hooge's law to a MOSFET

$1/f$ noise is often characterized using "Hooge's law", which is an *empirical* relation that reads as follows:

$$S_I = \alpha_{\mathrm{H}} \cdot \frac{I^2}{\mathcal{N}} \cdot \frac{1}{f} \tag{37}$$

where α_{H} is the Hooge constant and $\mathcal{N}$ is the total number of charge carriers.
We will now evaluate Hooge's law for a MOSFET, following Ref. [17]. Consider a segment Δx of the channel, containing $\Delta\mathcal{N}$ charge carriers. Applying Hooge's law to this channel segment gives:

$$S_{\Delta I}(x, f) = \alpha_{\mathrm{H}} \cdot \frac{I_{\mathrm{DS}}^2}{\Delta\mathcal{N}} \cdot \frac{1}{f} \tag{38}$$

The integration from source to drain is performed according to Eq. 35. Thus we assume that the current noise sources associated with each channel segment are uncorrelated. Now we arrive at:

$$S_I = \frac{\alpha_{\mathrm{H}} I_{\mathrm{DS}}}{f L^2} \cdot \int_0^L \frac{I_{\mathrm{DS}} \Delta x \mathrm{d}x}{\Delta\mathcal{N}} \tag{39}$$

Now we use that $\Delta\mathcal{N} = -W Q_{\mathrm{i}}(x) \Delta x / q$, and $I_{\mathrm{DS}} = -W \mu_{\mathrm{eff}} Q_{\mathrm{i}}(x) \frac{\mathrm{d}V}{\mathrm{d}x}$ [i.e. Eqs. (23) and (24)]:

$$S_I = \frac{\alpha_{\mathrm{H}} q I_{\mathrm{DS}} \mu_{\mathrm{eff}}}{f L^2} \cdot \int_0^L \frac{\mathrm{d}V}{\mathrm{d}x} \mathrm{d}x \tag{40}$$

This finally leads to:

$$\boxed{S_I = \alpha_{\mathrm{H}} \cdot \frac{q \mu_{\mathrm{eff}} I_{\mathrm{DS}} V_{\mathrm{DS}}}{f L^2}} \tag{41}$$

The above formula should be valid both in subthreshold and strong inversion.
A simple formula for the strong inversion regime is obtained if we use the basic drain current expression

$$I_{\mathrm{DS}} = \mu_{\mathrm{eff}} C_{\mathrm{ox}} \frac{W}{L} (V_{\mathrm{GT}} - \frac{1}{2} V_{\mathrm{DS}}) \cdot V_{\mathrm{DS}} \tag{42}$$

Now we find for the input referred voltage noise in strong inversion:

$$S_{V_{\mathrm{gate}}} = \frac{\alpha_{\mathrm{H}} q (V_{\mathrm{GT}} - \frac{1}{2} V_{\mathrm{DS}})}{W L C_{\mathrm{ox}} f} \tag{43}$$

This result is sometimes referred to as the 'Kleinpenning model'. Usually it is assumed that the contribution of the pinch-off region is negligible, as confirmed by the experiments (see Fig. 16). Then, in saturation we can simply replace V_{DS} in the above formula by $V_{\mathrm{DSAT}} \approx V_{\mathrm{GT}}$, so that:

$$S_{V_{\mathrm{gate}}} = \frac{\alpha_{\mathrm{H}} q V_{\mathrm{GT}}}{2 W L C_{\mathrm{ox}} f} \tag{44}$$

©Philips Electronics N.V. 1998

©Philips Electronics N.V. 1998

B The level 903 $1/f$ noise model

B.1 Derivation of the model by Hung *et al.*

In this section, we will elucidate the mathematical derivation of the new $1/f$ noise model. This is not meant to be exhaustive, but meant to give the reader an idea how the seemingly difficult formulae of this model come about. For a full derivation we refer to the original papers [9, 10].
The derivation starts with a calculation of the fluctuations in the number of occupied traps at a position x in the channel (x is the direction from source to drain). According to conventional number fluctuation theory this is given by:

$$S_{\Delta N_{\mathrm{t}}}(x,f) = \int_{E_{\mathrm{v}}}^{E_{\mathrm{c}}}\int_{0}^{W}\int_{0}^{t_{\mathrm{ox}}} 4n_{\mathrm{t}}(E,x,y,z)\,\Delta x\, f_{\mathrm{FD}}(1-f_{\mathrm{FD}})\,\frac{\tau}{1+4\pi^2 f^2\tau^2}\,\mathrm{d}z\,\mathrm{d}y\,\mathrm{d}E \tag{45}$$

Integration has to be performed over the different trap depths z, over the various trap energies E, and finally over the channel width W (i.e. the y direction). It is assumed that the distribution of traps is spatially uniform (i.e. $n_{\mathrm{t}}(E,x,y,z) = n_{\mathrm{t}}(E)$). The factor $f_{\mathrm{FD}}(1-f_{\mathrm{FD}})$ expresses that a trapping process can only take place from a filled state to a non-filled state or vice versa ($f_{\mathrm{FD}} = [1+\exp(E-E_{\mathrm{fn}}))/k_{\mathrm{B}}T]^{-1}$ is the Fermi-Dirac trap occupancy function). Because $f_{\mathrm{FD}}(1-f_{\mathrm{FD}})$ behaves like a delta function around the quasi-Fermi level, $n_{\mathrm{t}}(E)$ can be replaced by $n_{\mathrm{t}}(E_{\mathrm{fn}})$ and taken out of the integral. The time constant τ is given by:

$$\tau = \tau_0(E)\cdot\exp(\gamma_{\mathrm{ox}} z) \tag{46}$$

where $\tau_0(E)$ is the time constant at the interface and γ_{ox} is the attenuation coefficient of the electron wave function in the gate oxide. For $t_{\mathrm{ox}} \gg 1/\gamma_{\mathrm{ox}}$ and $f \ll 1/(2\pi\tau_0(E))$, the integration over z and y yields:

$$S_{\Delta N_{\mathrm{t}}}(x,f) = \frac{n_{\mathrm{t}}(E_{\mathrm{fn}})\Delta x W}{\gamma_{\mathrm{ox}} f}\cdot\int_{E_{\mathrm{v}}}^{E_{\mathrm{c}}} f_{\mathrm{FD}}(1-f_{\mathrm{FD}})\,\mathrm{d}E \tag{47}$$

Now the integration over the energy E has to be performed. This is facilitated using the equality

$$f_{\mathrm{FD}}(1-f_{\mathrm{FD}}) = -k_{\mathrm{B}}T\cdot\frac{\mathrm{d}f_{\mathrm{FD}}}{\mathrm{d}E} \tag{48}$$

Using $f_{\mathrm{FD}}(E_{\mathrm{c}})\approx 0$ and $f_{\mathrm{FD}}(E_{\mathrm{v}})\approx 1$ one arrives at:

$$S_{\Delta N_{\mathrm{t}}}(x,f) \approx n_{\mathrm{t}}(E_{\mathrm{fn}})\,\frac{k_{\mathrm{B}}T\,W\Delta x}{\gamma_{\mathrm{ox}}\,f} \tag{49}$$

Now that we know the fluctuations in the number of occupied traps at position x in the channel, we are interested in their effect on the drain current I_{DS}. As explained

©Philips Electronics N.V. 1998

in the Sec. 3, the fluctuations of mobility and carrier number are correlated. This leads to [10]:

$$S_{I,\Delta x}(x,f) = S_{\Delta N_\mathrm{t}}(x,f)\left[\frac{I_\mathrm{DS}}{NW\Delta x}(R \pm \alpha_\mathrm{S}\mu_\mathrm{eff}N)\right]^2 \tag{50}$$

Here, N is the carrier density, μ_eff is the effective mobility, and α_S is a scattering coefficient, responsible for the mobility fluctuations. It has been found from independent measurements that α_S is typically 10^{-15} Vs, and that its value decreases with increasing carrier density due to screening effects. Furthermore, the ratio R is introduced, defined as:

$$R \equiv \frac{\partial \Delta N}{\partial \Delta N_\mathrm{t}} \tag{51}$$

This ratio R can be expressed as:

$$R = -\frac{C_\mathrm{i}}{C_\mathrm{ox} + C_\mathrm{i} + C_\mathrm{d} + C_\mathrm{it}} \tag{52}$$

where C_ox, C_i, C_d and C_it are the oxide, inversion layer, depletion layer, and interface trap capacitances, respectively. Using $C_\mathrm{i} \approx \frac{q^2}{k_\mathrm{B}T}N$, this can be rewritten as

$$R = -\frac{N}{N + N^*} \tag{53}$$

with

$$N^* = \frac{k_B T}{q^2}(C_\mathrm{ox} + C_\mathrm{d} + C_\mathrm{it}) \tag{54}$$

Note that R approaches -1 in strong inversion.
Now we are ready to perform the integration over the channel length. Assuming that the current noise sources in each part Δx of the channel are uncorrelated, the correct method to calculate the total noise in the drain current is:

$$S_I(f) = \frac{1}{L^2}\int_0^L S_{I,\Delta x}(x,f)\,\Delta x\,\mathrm{d}x \tag{55}$$

This formula is not trivial. The derivation, after van der Ziel, is shown in appendix A. Combining Eqs. (50) and (55) leads to:

$$S_I(f) = \frac{k_\mathrm{B}TI_\mathrm{DS}^2}{\gamma_\mathrm{ox}fWL^2}\int_0^L n_\mathrm{t}(E_\mathrm{fn})\left[\frac{R}{N(x)} \pm \alpha_\mathrm{S}\mu_\mathrm{eff}\right]^2 \mathrm{d}x \tag{56}$$

Just as in the derivation of IV models, it is convenient to replace the integration over x by integration over the quasi-Fermi potential V, using Eqs. (23) and (24), which leads to

$$S_I(f) = \frac{k_\mathrm{B}\,T\,q\,I_\mathrm{DS}\,\mu_\mathrm{eff}}{\gamma_\mathrm{ox}\,f\,L^2}\int_0^{V_\mathrm{DS}} n_\mathrm{t}(E_\mathrm{fn})\,\frac{R^2}{N}(1 \pm \alpha_\mathrm{S}\mu_\mathrm{eff}\frac{N}{R})^2\,\mathrm{d}V \tag{57}$$

 ©Philips Electronics N.V. 1998

To proceed further, one needs to know the bias dependence of $\alpha_{\rm S}$, $\mu_{\rm eff}$, and $n_{\rm t}(E_{\rm fn})$. In order to keep things mathematically feasible, the following parametrization is made:

$$n_{\rm t}(E_{\rm fn})(1 \pm \alpha_{\rm S}\mu_{\rm eff}\frac{N}{R})^2 = A + BN + CN^2 \tag{58}$$

Using $qN(x) = C_{\rm ox} \cdot [V_{\rm GT} - aV(x)]$ one can replace the integration over V by integration over N. Here a is the factor that corrects for the variation of the depletion region depth going from source to drain, i.e. $(1+\delta_1)$ in MOS Model 9. In the linear regime, we arrive at:

$$S_I(f) = \frac{k_{\rm B}Tq^2 I_{\rm DS}\mu_{\rm eff}}{a\gamma_{\rm ox} f L^2 C_{\rm ox}}\left[A\ln\frac{N_0+N^*}{N_L+N^*} + B(N_0-N_L) + \frac{1}{2}C(N_0^2-N_L^2)\right] \tag{59}$$

where N_0 and N_L are the charges at the source and drain end of the channel, respectively:

$$N_0 = \frac{C_{\rm ox}}{q}\cdot V_{\rm GT} \tag{60}$$

and

$$N_L = \frac{C_{\rm ox}}{q}\cdot (V_{\rm GT} - aV_{\rm DS}) \tag{61}$$

In saturation, there is an additional contribution of the pinch-off region. We will not show the derivation here. According to Refs. [9, 10] the expression for the drain current flicker noise now reads:

$$S_I(f) = \frac{k_{\rm B}Tq^2 I_{\rm DS}\mu_{\rm eff}}{a\gamma_{\rm ox} f L^2 C_{\rm ox}}\left[A\ln\frac{N_0+N^*}{N_L+N^*} + B(N_0-N_L) + \frac{1}{2}C(N_0^2-N_L^2)\right] + \Delta L \cdot \frac{k_{\rm B}TI_{\rm DS}^2}{\gamma_{\rm ox} f W L^2}\cdot\frac{A+BN_{\rm L}+CN_{\rm L}^2}{(N_{\rm L}+N^*)^2} \tag{62}$$

In the subthreshold region, the noise turns out to be:

$$S_I(f) = \frac{Ak_{\rm B}TI_{\rm DS}^2}{WL\gamma_{\rm ox} f {N^*}^2} \tag{63}$$

Here, terms with B and C are neglected.

B.2 Rewriting Hung's model in MOS Model 9 terms

Now we will show how we have rewritten the model by Hung *et al.* in MOS Model 9 terms. First, the factor $a = 1 + \delta_1$ is dropped from Eqs. (61) and (62). We have made this approximation to keep our model compatible with the BSIM3v3 implementation [11], which makes the same approximation. This has, however, quite some effect on the magnitude of the calculated noise, as shown in Fig. 17.

©Philips Electronics N.V. 1998

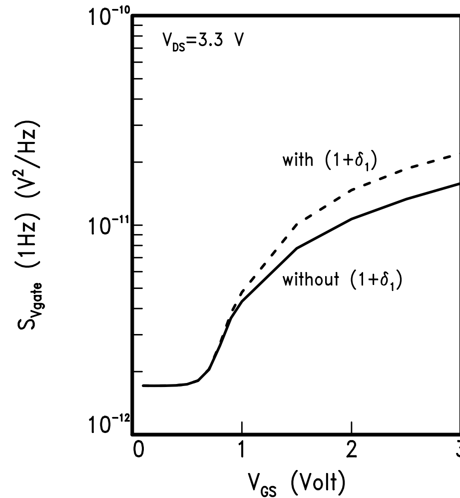

Figure 17: Example of the effect of dropping $(1+\delta_1)$ from the model equations.

Next we write $C_{\rm ox} = \frac{\epsilon_{\rm ox}}{t_{\rm ox}}$, because in MOS Model 9, $C_{\rm ox}$ has the meaning of the *total* oxide capacity (in F), and not the specific oxide capacity (in F/m^2) that we need here. Because we do not want W and L to appear on the miniset level, we solved this by making $t_{\rm ox}$ a miniset parameter.
Now the expressions (60) and (61) for the charges at the source and drain ends of the channel become:

$$N_0 = \frac{\epsilon_{\rm ox}}{q t_{\rm ox}} \cdot V_{\rm GT3} \tag{64}$$

and

$$N_{\rm L} = \frac{\epsilon_{\rm ox}}{q t_{\rm ox}} \cdot (V_{\rm GT3} - V_{\rm DS1}) \tag{65}$$

Now we will rewrite the prefactor in Eq. (59). First we note that

$$\mu_{\rm eff} = \frac{\mu_0}{\{1 + \theta_1 V_{\rm GT1} + \theta_2 \cdot (u_{\rm s} - u_{\rm s0})\}} \tag{66}$$

Note that there is no velocity saturation (θ_3) in the model, just as in the original model by Hung *et al.* and its BSIM implementation. Now we introduce the MOS Model 9 gain factor β:

$$\beta = \mu_0 C_{\rm ox} \frac{W}{L} \tag{67}$$

and, again using $C_{\rm ox} = \frac{\epsilon_{\rm ox}}{t_{\rm ox}}$, arrive at

$$\frac{k_{\rm B} T q^2 I_{\rm DS} \mu_{\rm eff}}{\gamma_{\rm ox} f L^2 C_{\rm ox}} = \frac{\phi_{\rm T} q^2 I_{\rm DS} \beta}{f \epsilon_{\rm ox}^2 \{1 + \theta_1 V_{\rm GT1} + \theta_2 \cdot (u_{\rm s} - u_{\rm s0})\}} \cdot \frac{q}{\gamma_{\rm ox} W_{\rm E} L_{\rm E}} \tag{68}$$

 ©Philips Electronics N.V. 1998

Note that we replaced the drawn channel dimensions W and L by the electrical dimensions $W_{\rm E}$ and $L_{\rm E}$. Now we introduce the MOS Model 9 noise parameters $N_{\rm FA}$, $N_{\rm FB}$, and $N_{\rm FC}$:

$$\begin{aligned} N_{\rm FA} &= A \cdot \frac{q}{\gamma_{\rm ox} L_{\rm E} W_{\rm E}} \\ N_{\rm FB} &= B \cdot \frac{q}{\gamma_{\rm ox} L_{\rm E} W_{\rm E}} \\ N_{\rm FC} &= C \cdot \frac{q}{\gamma_{\rm ox} L_{\rm E} W_{\rm E}} \end{aligned} \tag{69}$$

Therefore in strong inversion, the 1/f noise spectral density, denoted by $S_{\rm si}$, expressed in MM9 terms, reads:

$$\begin{aligned} S_{\rm si} = {} & \frac{\phi_{\rm T}\, q^2 I_{\rm DS}\, \beta\, t_{\rm ox}^2}{f \epsilon_{\rm ox}^2 \left\{1 + \theta_1 V_{\rm GT1} + \theta_2 \cdot (u_{\rm s} - u_{\rm s0})\right\}} \times \\ & \left[N_{\rm FA} \cdot \ln \frac{N_0 + N^*}{N_{\rm L} + N^*} + N_{\rm FB} \cdot (N_0 - N_{\rm L}) + \frac{1}{2} \cdot N_{\rm FC} \cdot (N_0^2 - N_{\rm L}^2) \right] \end{aligned} \tag{70}$$

Now we need to rewrite the pinch-off term. Therefore we need an expression for the channel-length-modulation ΔL in MOS Model 9 terms. In case of pinch-off, the drain current is proportional to:

$$\frac{W_{\rm E}}{L_{\rm E} - \Delta L} = \frac{W_{\rm E}}{L_{\rm E}} \cdot \frac{1}{1 - \frac{\Delta L}{L_{\rm E}}} \equiv \frac{W_{\rm E}}{L_{\rm E}} \cdot G_2 \tag{71}$$

where $G_2 = 1/(1 + (\Delta L/L_{\rm E}))$ is the MOS Model 9 factor describing channel length modulation (see Eq. (2.25) in Ref. [2]). Now we see that we may write:

$$\frac{\Delta L}{L_{\rm E}} = \frac{G_2 - 1}{G_2} \tag{72}$$

Note that we have $\Delta L = 0$ when $G_2 = 1$, as expected. Now the full expression for the noise in the saturation region is readily found to be:

$$\begin{aligned} S_{\rm si} = {} & \frac{\phi_{\rm T}\, q^2 I_{\rm DS}\, \beta\, t_{\rm ox}^2}{f \epsilon_{\rm ox}^2 \left\{1 + \theta_1 V_{\rm GT1} + \theta_2 \cdot (u_{\rm s} - u_{\rm s0})\right\}} \times \\ & \left[N_{\rm FA} \cdot \ln \frac{N_0 + N^*}{N_{\rm L} + N^*} + N_{\rm FB} \cdot (N_0 - N_{\rm L}) + \frac{1}{2} \cdot N_{\rm FC} \cdot (N_0^2 - N_{\rm L}^2) \right] \\ & + \frac{\phi_{\rm T}\, I_{\rm DS}^2}{f} \cdot \frac{G_2 - 1}{G_2} \cdot \left[\frac{N_{\rm FA} + N_{\rm FB} N_{\rm L} + N_{\rm FC} N_{\rm L}^2}{(N_{\rm L} + N^*)^2} \right] \end{aligned} \tag{73}$$

Similarly, we rewrite the 1/f noise spectral density in weak inversion, denoted by $S_{\rm wi}$:

$$S_{\rm wi} = \frac{A k_{\rm B} T I_{\rm DS}^2}{W L \gamma_{\rm ox} f N^{*2}} = N_{\rm FA} \cdot \frac{\phi_{\rm T} I_{\rm DS}^2}{f N^{*2}} \tag{74}$$

©Philips Electronics N.V. 1998

B.3 The transition between weak and strong inversion

So far, we have shown separate expressions for S_{wi} and S_{si}, the flicker noise in the weak and strong inversion regimes. In the BSIM3v3 model the flicker noise S_{fl} in the drain current is calculated as follows:

$$\begin{aligned} \text{if } V_{\mathrm{GT}} > 0.1\ \mathrm{V}\ \text{then}: &\quad S_{\mathrm{fl}} = S_{\mathrm{si}} \\ \text{else}: &\quad S_{\mathrm{fl}} = \frac{S_{\mathrm{si}}(V_{\mathrm{GT}} = 0.1\ \mathrm{V}) \times S_{\mathrm{wi}}}{S_{\mathrm{si}}(V_{\mathrm{GT}} = 0.1\ \mathrm{V}) + S_{\mathrm{wi}}} \end{aligned} \tag{75}$$

This transition is not very smooth, as depicted in the left frame of Fig. 18. Therefore we improved this transition for the MOS Model 9 implementation of the model:

$$S_{\mathrm{fl}} = \frac{S_{\mathrm{si}} \times S_{\mathrm{wi}}}{S_{\mathrm{si}} + S_{\mathrm{wi}}} \tag{76}$$

As shown in the right frame of Fig. 18, this transition has indeed been smoothed. Moreover, our expression for S_{fl} approaches the S_{wi} line much better in the weak inversion regime.

Note that this transition has the consequence that the parameter N_{FA} has to be non-zero. This is because if $N_{\mathrm{FA}} = 0$, the noise in weak inversion S_{wi} becomes zero as well, see Eq. (74). The final result S_{fl}, in turn, see Eq. (76), will also vanish.

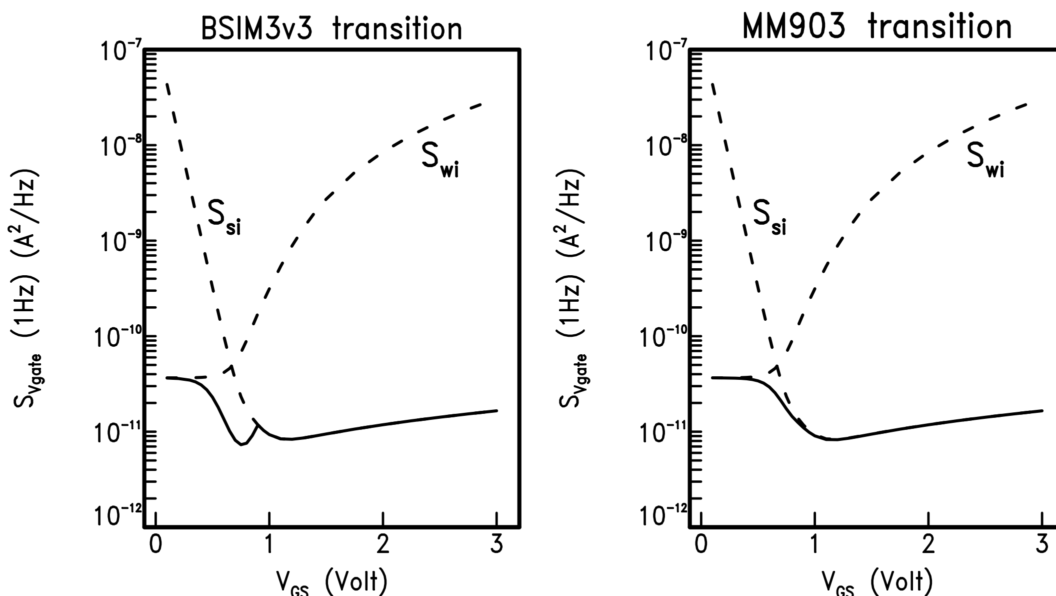

Figure 18: The transition from weak to strong inversion in the BSIM3v3 model (*left*) and in MOS Model 903 (*right*).

 ©Philips Electronics N.V. 1998

B.4 The value of N^*

Now we rewrite the expression for N^* in MOS Model 9 terms using the well-known relation $m = m_0 + 1 = (C_{\rm ox} + C_{\rm d} + C_{\rm it})/C_{\rm ox}$. This leads to:

$$N^* = \frac{\epsilon_{\rm ox}}{q t_{\rm ox}} \cdot \phi_{\rm T} \cdot (m_0 + 1) \tag{77}$$

Note that this differs from the BSIM3v3 implementation, where this N^* has been changed into a fixed parameter: $N^* = 2 \times 10^{14}\ {\rm m}^{-2}$. We do not know the reason for this.
We have implemented Eq. (77) in MOS Model 9, because this turned out to give better modelling results than setting $N^* = 2 \times 10^{14}\ {\rm m}^{-2}$. This is illustrated in Fig. 19. In the BSIM implementation a 'dip' appears in the noise intensity as a function of $V_{\rm GS}$ near $V_{\rm TO}$. In our implementation, the curve is more or less flat around and beneath $V_{\rm TO}$, much more in accordance with our data.

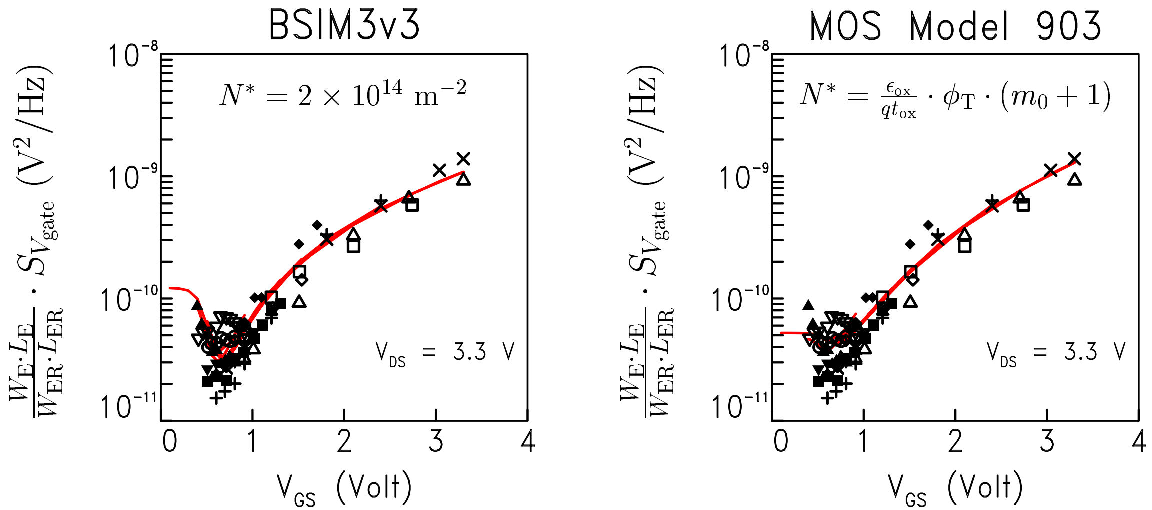

Figure 19: Comparison of the BSIM3v3 and the MOS model 9 expressions for N^*. Different data points correspond to 11 different PMOS geometries, see Sec. 4.

B.5 Scaling rules

We have introduced the three (miniset) noise parameters $N_{\rm FA}$, $N_{\rm FB}$, and $N_{\rm FC}$ in Eq. (69). Rewriting these expressions in MOS Model 9 fashion we get:

$$\begin{aligned} N_{\rm FA} &= \frac{W_{\rm ER} L_{\rm ER}}{W_{\rm E} L_{\rm E}} \cdot N_{\rm FAR} \\ N_{\rm FB} &= \frac{W_{\rm ER} L_{\rm ER}}{W_{\rm E} L_{\rm E}} \cdot N_{\rm FBR} \end{aligned} \tag{78}$$

©Philips Electronics N.V. 1998

$$N_{\mathrm{FC}} = \frac{W_{\mathrm{ER}} L_{\mathrm{ER}}}{W_{\mathrm{E}} L_{\mathrm{E}}} \cdot N_{\mathrm{FCR}}$$

where we have introduced the maxiset noise parameters N_{FAR}, N_{FBR}, and N_{FCR}. Note that the geometrical scaling rules of the model parameters are identical to that of N_{FR} in MOS MODEL 9, level 902. In fact, most $1/f$ noise models, have the same geometrical scaling:

$$S_{V_{\mathrm{gate}}} \propto \frac{1}{W_{\mathrm{E}} L_{\mathrm{E}}} \quad \text{(approximately)} \tag{79}$$

The three new noise parameters on the maxiset level are N_{FAR}, N_{FBR}, N_{FCR}. These are related to the A, B, and C introduced in Eq. (58) by:

$$N_{\mathrm{FAR}} = A \cdot \frac{q}{\gamma_{\mathrm{ox}} L_{\mathrm{ER}} W_{\mathrm{ER}}} \tag{80}$$

$$N_{\mathrm{FBR}} = B \cdot \frac{q}{\gamma_{\mathrm{ox}} L_{\mathrm{ER}} W_{\mathrm{ER}}} \tag{81}$$

$$N_{\mathrm{FCR}} = C \cdot \frac{q}{\gamma_{\mathrm{ox}} L_{\mathrm{ER}} W_{\mathrm{ER}}} \tag{82}$$

Finally we note that there are no explicit temperature scaling rules of the parameters. However, the model equations have an implicit temperature dependence via ϕ_{T} ($\equiv k_{\mathrm{B}} T/q$).

B.6 Simplified model and physical interpretation of the parameters

If we simplify the model, following Ref. [18], a physical interpretation of the new noise parameters can be given. This simplification neglects the dependences of $n_{\mathrm{t}}(E_{\mathrm{fn}})$, α_{S}, and μ_{eff} on carrier density N. Doing so, combination of Eqs. (58), (80), (81), (82) gives us the following physical interpretation of the noise parameters:

$$N_{\mathrm{FAR}} = n_{\mathrm{t}} \cdot \frac{q}{\gamma_{\mathrm{ox}} L_{\mathrm{ER}} W_{\mathrm{ER}}} \tag{83}$$

$$N_{\mathrm{FBR}} = 2\alpha_{\mathrm{S}} \mu_{\mathrm{eff}} N_{\mathrm{FAR}} \tag{84}$$

$$N_{\mathrm{FCR}} = \frac{N_{\mathrm{FBR}}^2}{4 N_{\mathrm{FAR}}} \tag{85}$$

Thus from the parameter N_{FAR} an “average” trap density n_{t} can be calculated. For NMOS, one typically finds $N_{\mathrm{FAR}} \sim 10^{24}\mathrm{V}^{-1}\mathrm{m}^{-4}$ corresponding to $n_{\mathrm{t}} = 2 \times 10^{41}\mathrm{m}^{-3}\mathrm{J}^{-1}$. Next, an “average” scattering coefficient α_{S} can be derived from N_{FBR}. For a typical value $N_{\mathrm{FBR}} \sim 10^{8}\mathrm{V}^{-1}\mathrm{m}^{-2}$ and $\mu_{\mathrm{eff}} = 0.04\mathrm{m}^2/\mathrm{Vs}$ we arrive at $\alpha_{\mathrm{S}} = 10^{-15}$ Vs. Note that in this simplified model N_{FCR} is not a free parameter anymore but follows directly from N_{FAR}, N_{FBR}. Thus if one is really interested in deriving values for n_{t} and α_{S} from $1/f$ noise measurements, it makes sense to extract the noise parameters under the constraint (85), as proposed in Ref. [18].

Note that in MOS Model 9, we do not *use this simplified model, and we do* not *recommend it for the purpose of compact modelling for circuit simulation.*

 ©Philips Electronics N.V. 1998

B.7 Hooge's law

The situation where the term with N_{FB} is the dominant term is of special interest. This is the case when mobility scattering is the dominant mechanism, and N_{FC} is not too big. In such a case, Eq. (59) in strong inversion simplifies to:

$$S_{\mathrm{si}} = (N_{\mathrm{FBR}} \cdot L_{\mathrm{ER}} \cdot W_{\mathrm{ER}} \cdot \phi_{\mathrm{T}}) \cdot \frac{q\mu_{\mathrm{eff}} I_{\mathrm{DS}} V_{\mathrm{DS}}}{f L^2} \tag{86}$$

This is exactly the same equation that we found in Appendix A by applying Hooge's law to a MOSFET, see Eq. (43), if we take the Hooge constant α_{H} to be equal to:

$$\alpha_{\mathrm{H}} = N_{\mathrm{FBR}} \cdot L_{\mathrm{ER}} \cdot W_{\mathrm{ER}} \cdot \phi_{\mathrm{T}} \tag{87}$$

Applying this to the values of N_{FBR} found in our parameter extraction, we find for α_{H} values of $\sim 10^{-5}$ for NMOS and $\sim 10^{-6}$ for PMOS devices.

©Philips Electronics N.V. 1998

 ©Philips Electronics N.V. 1998

C List of used symbols

Here we list the symbols used in this report, first the Greek symbols and then the Roman symbols.

symbol	description	unit
α_{H}	Hooge constant	–
α_{S}	scattering coefficient	Vs
β	MOS Model 9 gain factor (miniset parameter)	$\mathrm{A/V^2}$
γ	frequency exponent of flicker noise	–
γ_{ox}	attenuation coefficient of electron wave function in gate oxide	$\mathrm{m^{-1}}$
$\delta(x'-x)$	Dirac delta-function	$\mathrm{m^{-1}}$
δ_1	accounts for depletion layer depth variation from source to drain	–
ΔL	length of pinch-off region in saturation	m
ϵ_{ox}	absolute permittivity of gate oxide	F/m
θ_1	MOS Model 9 mobility reduction parameter (gate field)	$\mathrm{V^{-1}}$
θ_2	MOS Model 9 mobility reduction parameter (bulk field)	$\mathrm{V^{-\frac{1}{2}}}$
θ_3	MOS Model 9 mobility reduction parameter (velocity saturation)	$\mathrm{V^{-1}}$
μ_{eff}	effective mobility, defined by Eq. (66)	$\mathrm{m^2V^{-1}s^{-1}}$
μ_0	zero-field mobility	$\mathrm{m^2V^{-1}s^{-1}}$
τ	time constant of a trap	s
τ_0	time constant of a trap at the $\mathrm{Si/SiO_2}$ interface	s
ϕ_{B}	surface potential in strong inversion	V
ϕ_{T}	thermal voltage $\equiv k_{\mathrm{B}}T/q$	V
a	used in Refs. [9, 10], corresponds to $(1+\delta_1)$ in MOS Model 9	–
C_{d}	depletion layer capacitance per area	$\mathrm{F/m^2}$
C_{i}	inversion layer capacitance per area	$\mathrm{F/m^2}$
C_{it}	interface traps capacitance per area	$\mathrm{F/m^2}$
C_{ox}	specific oxide capacitance	$\mathrm{F/m^2}$
E	energy level	J
E_{fn}	quasi-Fermi level of electrons	J
f	frequency	Hz
f_{FD}	Fermi-Dirac occupancy function	–
F	noise figure	–
$\mathcal{F}(x,f)$	see Eq. (34)	$\mathrm{A^2m/Hz}$
$\mathcal{G}$	carrier generation rate	$\mathrm{s^{-1}}$
g_{m}	transconductance	A/V
$g(x)$	local conductivity, see Eqs. (23) and (24).	Ωm
G_2	MOS Model 9 factor describing channel length modulation	–
$h(x,t)$	fluctuating current inside the device	A
$i_{1/f}$	flicker noise current	A
I	current	A
I_{DS}	current flowing from source to drain	A
k_{B}	Boltzmann constant	$\mathrm{JK^{-1}}$

©Philips Electronics N.V. 1998

symbol	description	unit
L	drawn device length	m
$L_{\rm E}$	effective device length	m
$L_{\rm ER}$	effective device length of reference transistor	m
m_0	MOS Model 9 miniset parameter related to subthreshold slope	–
m	MOS Model 9 quantity, given by Eq. (2.14) in Ref. [2]	–
$n_{\rm t}$	number of traps per volume and per energy	$\rm m^{-3}J^{-1}$
N	density of charge carriers	$\rm m^{-2}$
$N_{\rm t}$	density of occupied traps	$\rm m^{-2}$
N_0	density of charge carriers at the source end of the channel	$\rm m^{-2}$
N_L	density of charge carriers at the drain end of the channel	$\rm m^{-2}$
N^*	abbreviation introduced in Eq. (54)	$\rm m^{-2}$
$N_{\rm F}$	flicker noise miniset parameter of MOS Model 902	$\rm V^2$
$N_{\rm FA}$	first flicker noise miniset parameter of new model	$\rm V^{-1}m^{-4}$
$N_{\rm FB}$	second flicker noise miniset parameter of new model	$\rm V^{-1}m^{-2}$
$N_{\rm FC}$	third flicker noise miniset parameter of new model	$\rm V^{-1}$
$N_{\rm FR}$	value of $N_{\rm F}$ for reference transistor	$\rm V^2$
$N_{\rm FAR}$	value of $N_{\rm FA}$ for reference transistor	$\rm V^{-1}m^{-4}$
$N_{\rm FBR}$	value of $N_{\rm FB}$ for reference transistor	$\rm V^{-1}m^{-2}$
$N_{\rm FCR}$	value of $N_{\rm FC}$ for reference transistor	$\rm V^{-1}$
NFMOD	switch in MOS Model 903 to select $1/f$ noise model	–
Noia	first BSIM3v3 flicker noise parameter	$\rm V^{-1}m^{-3}$
Noib	second BSIM3v3 flicker noise parameter	$\rm V^{-1}m^{-1}$
Noic	third BSIM3v3 flicker noise parameter	$\rm V^{-1}m$
$\mathcal{N}$	total number of charge carriers	–
q	elementary charge	C
$Q_{\rm i}$	inversion charge density	$\rm C/m^2$
$\mathcal{R}$	carrier recombination rate	$\rm s^{-1}$
R	ratio of fluctuations in N and $N_{\rm t}$	–
$R_{\rm meas}$	resistance value of measurement resistor	Ω
$S_{\rm fl}$	drain current $1/f$ noise in MOS Model 9	$\rm A^2/Hz$
$S_h(x,x',f)$	spatial cross-spectral intensity of $h(x,t)$	$\rm A^2/Hz$
$S_{\rm si}$	drain current $1/f$ noise in strong inversion	$\rm A^2/Hz$
$S_{\rm wi}$	drain current $1/f$ noise in weak inversion	$\rm A^2/Hz$
S_I	drain current noise	$\rm A^2/Hz$
$S_{I,\Delta x}(x,f)$	drain current noise of channel segment between x and $x+\Delta x$	$\rm A^2/Hz$
$S_{V_{\rm gate}}$	input-referred voltage noise	$\rm V^2/Hz$
$S_{V,\Delta x}(x,f)$	voltage noise of channel segment between x and $x+\Delta x$	$\rm V^2/Hz$
$S_{\Delta N_{\rm t}}$	spectral density of the fluctuations in $N_{\rm t}$	1/Hz
T	absolute temperature	K
$t_{\rm ox}$	oxide thickness (MOS Model 9 parameter)	m
$u_{\rm s}$	$\sqrt{V_{\rm SB}+\phi_{\rm B}}$	$\rm V^{\frac{1}{2}}$
$u_{\rm s0}$	$\sqrt{V_{\rm SB}}$	$\rm V^{\frac{1}{2}}$

 ©Philips Electronics N.V. 1998

symbol	**description**	**unit**
$v_{1/f}$	flicker noise voltage	V
V	externally applied voltage or quasi-Fermi-potential of the charge carriers	V
V_{D}	voltage at the drain	V
V_{DS}	drain-source voltage	V
V_{GS}	gate-source voltage	V
V_{SB}	source-bulk voltage	V
V_{GT}	gate drive $V_{\mathrm{GS}} - V_{\mathrm{TO}}$	V
V_{GT1}	gate drive; see Ref. [2], Eq.(2.9)	V
V_{GT3}	gate drive; see Ref. [2], Eq.(2.26)	V
V_{TO}	MOS Model 9 threshold voltage	V
W	drawn device width	m
W_{E}	effective device width	m
W_{ER}	effective device width of reference transistor	m
x	direction from source to drain	m
y	direction along channel width	m
z	direction perpendicular to Si/SiO_2 interface	m

©Philips Electronics N.V. 1998

©Philips Electronics N.V. 1998

References

[1] MOS Model Book, Dec. 1996, Philips ED & T/Analogue Simulation.

[2] R.M.D.A. Velghe, D.B.M. Klaassen, F.M. Klaassen, MOS Model 9 , Nat. Lab. Unclassified Report NL-UR 003/94.

[3] Internet: `http://www.semiconductors.philips.com/Philips_Models`.

[4] J.A.M. de Boet and R.R.J. Vanoppen, *1/f noise characterization of C200 MOS transistors*, NL-TN 220/93;
1/f noise in buried/ surface channel PMOSFETs, 30-6-1994;
1/f noise characterization C100T5, unclassified RWR-JB-950222-jb, 22-2-1995;
1/f noise characterization Qubic Nmos, 25-6-1993;
Verkennende LF-ruis metingen aan C150LP Pmos transistoren, 5-1-1993.

[5] A.J. Scholten and D.B.M. Klaassen, *The thermal noise model in MOS Model 9*, in preparation.

[6] R. Vanoppen, *RF noise characterization*, NL-TN 134/97.

[7] A. van der Ziel, *Noise: sources, characterization, measurement*, Prentice-Hall, 1970.

[8] A. van der Ziel, *Noise in measurements*, John Wiley & Sons, 1976.

[9] Kwok K. Hung *et al.*, *A unified model for the flicker noise in metal-oxide-semiconductor field-effect transistors*, IEEE Trans El. Dev. Vol. 37, No. 3, March 1990.

[10] Kwok K. Hung *et al.*, *A physics-based MOSFET noise model for circuit simulators*, IEEE Trans El. Dev. Vol. 37, No. 5, May 1990.

[11] Yuhua Cheng *et al.*, *BSIM3v3 Manual*, 1996, available from `http://rely.eecs.berkeley.edu:8080/bsim3www`.

[12] A.J. Scholten and D.B.M. Klaassen, *Modelling of* $1/f$ *noise in MOSFETs*, BMMWP#11, November 26th, Philips Nat.Lab. Eindhoven.

[13] A.J. Scholten and D.B.M. Klaassen, *Modeling of* $1/f$ *noise for C075*, BMMWP#12, May 13th, Philips Nat.Lab. Eindhoven.

[14] G. Ghibaudo and O. Roux-dit-Buisson, *Low-frequency fluctuations in scaled down silicon CMOS devices status and trends*, Proc. ESSDERC '94, pp.693-700 (1994).

[15] F.M. Klaassen and J. Prins, *Thermal noise of MOS transistors*, Phil. Res. Repts. **22**, 504-514, 1967.

©Philips Electronics N.V. 1998

[16] K.M. van Vliet *et al.*, *Noise in single injection diodes. I. A Survey of methods*, Journal of Applied Physics, Vol. 46, No.4, April 1975, pp. 1804-1813.

[17] F.M. Klaassen, *Characterization of low* $1/f$ *noise in MOS transistors*, IEEE Trans. El. Dev., Vol. ED-18, no.10, october 1971.

[18] M. van Heijningen, E. Vandamme, L. Deferm, and L.Vandamme, *Modeling 1/f noise and extraction of the SPICE noise parameters using a new extraction procedure*, Proc. ESSDERC Conference '98.

 ©Philips Electronics N.V. 1998

Author(s) A.J. Scholten and D.B.M. Klaassen

Title New 1/f noise model in MOS Model 9, level 903

Distribution

Nat.Lab./PI	WB-5	
PRL	Redhill, UK	
PRB	Briarcliff Manor, USA	
LEP	Limeil–Brévannes, France	
PFL	Aachen, BRD	
CP&T	WAH	
Adjunct-directeur:	Ir. M.G. Collet	WAG-14
Groepsleider:	Dr. R. Woltjer	WAG-14

Abstract

S. McIntosh	COO office	BAE-2
A. van Gorkum	CTO office	BAE-2
T. Claasen	CTO office	BAE-2
J. Lohstroh	CTO office	BAE-2
T. Akkermans	Chief Strategy Officer	BAE-2
G. Groenendaal	SPM telecom	BAE-2
J. Verhoeks	SPMM C-IC	BAE-2
J.B. Theeten	SPMM C-IC	BAE-2
E. Odijk	SPMM C+M	BAE-2
R. v.d. Bij	SPMM Discrete	BAE-4
J. Bloos	SPMM Discrete	BAE-4
R. Sykes	SPMM ASL	Sunnyvale
A. Reader	46 Impasse des Buis, 38920	Crolles, France
P. Coppelmans	S&V IC Lab.	SFJ-6
R. Kluitmans	CE.IC Lab	SFJ-658
R. Braam	CE.IC Lab	SFJ-6
W. Leising	CIC	Hamburg LA 351
J. Meeuwis	PCALE CAD Support Group	BE-505
H. van Glabbeek	PCAL-E	BE-4
H. Otten	SLE	BE-5
H. Okel	Philips RHW	Hamburg
J. Fock	Philips RHW	Hamburg
G. Sieboerger	Philips RHW	Hamburg
J. Lebailly	Philips Composants	Caen
J. Journeau	Philips Composants	Caen

©Philips Electronics N.V. 1998

C. Biard	Philips Composants	Caen
E. Weagel	Philips Semiconductors	Albuquerque
N. Hoffman	Philips Semiconductors	BAE-2
L. Gambus	Philips Semiconductors	Caen
M. Bolt	Philips Semiconductors	Crolles
H. Grabe	Philips Semiconductors	Hamburg
T. Evelbauer	Philips Semiconductors	Hamburg
R. Grover	Philips Semiconductors	Hazel Grove
L. Gee	Philips Semiconductors	Southampton
B. Redman-White	Philips Semiconductors	Southampton
F. van Roosmalen	Philips Semiconductors	Stadskanaal
M. Shields	Philips Semiconductors	Sunnyvale
G. Conner	Philips Semiconductors	Sunnyvale
K. Davis	Philips Semiconductors	Sunnyvale
J. Hendrickx	Philips Semiconductors	WAY41
M. Locher	Philips Semiconductors	Zürich
J. Solo	Philips Semiconductors	Zürich
R. Penning de Vries	Philips Semiconductors	Nijmegen
W. Josquin	Philips Semiconductors	Nijmegen
A. Linssen	Philips Semiconductors	Nijmegen
M. Hillen	Philips Semiconductors	Nijmegen
H. Boezen	Philips Semiconductors	Nijmegen
J. Schmitz	Philips Semiconductors	Nijmegen
J. van der Pol	Philips Semiconductors	Nijmegen
G. de Groot	Philips Semiconductors	Nijmegen
Th. Smit	Philips Semiconductors	Nijmegen
H. van der Vlist	Philips Semiconductors	Nijmegen
M. Versleijen	Philips Semiconductors	Nijmegen
L. van de Hoven	Philips Semiconductors	Nijmegen
J. Bruines	Philips Semiconductors	Nijmegen
M. Berkhout	Philips Semiconductors	Nijmegen
M. van Dort	Philips Semiconductors	Nijmegen
J. Egbers	Philips Semiconductors	Nijmegen
P. Emonts	Philips Semiconductors	Nijmegen
L. Harm	Philips Semiconductors	Nijmegen
S. Nath	Philips Semiconductors	Nijmegen
R. Tuijtelaars	Philips Semiconductors	Nijmegen
J. Willms	Philips Semiconductors	Nijmegen
S. Onneweer	ED&T Analogue Simulation	WAY-31
H. Hermans	ED&T Analogue Simulation	WAY-31
J. Fijnvandraat	ED&T Analogue Simulation	WAY-31
M. Bennebroek	Philips Research	WAG-01
N. Cowern	Philips Research	WAG-01

 ©Philips Electronics N.V. 1998

C. de Graaf	Philips Research	WAG-13
R. Havens	Philips Research	WAG-12
E. van der Heijden	Philips Research	WAG-13
L. Huijten	Philips Research	WAG-04
B. Huizing	Philips Research	WAG-04
F. Hurkx	Philips Research	WAG-13
D. Klaassen	Philips Research	WAG-13
H. Kretschman	Philips Research	WAG-12
M. Peter	Philips Research	WAG-13
F. van Rijs	Philips Research	WAG-12
H. Schligtenhorst	Philips Research	WAG-13
J. Slotboom	Philips Research	WAG-12
M. Slotboom	Philips Research	WAG-01
P. Stolk	Philips Research	WAG-01
P. de Vreede	Philips Research	WAG-12
F. Widdershoven	Philips Research	WAM-01
J. Schmitz	Philips Research	WAG-12
A. Montree	Philips Research	WAG-03
C. van der Poel	Philips Research	WAG-14
M. Graef	Philips Research	WAG-14
J. van Gerwen	Philips Research	WAY-32
R. van de Grift	Philips Research	WAY-31
E. Roza	Philips Research	WAY-41
A. Sempel	Philips Research	WAY-51
C. Wouda	Philips Research	WAY-52
P. Meijer	Philips Research	WAY-41
J.B. Hughes	Philips Research	Redhill
M. Simpson	Philips Research	Briarcliff Manor

Full report

T. Smedes	Philips Semiconductors	Nijmegen
C. van Velthooven	Philips Semiconductors	Nijmegen
W. Nijland	Philips Semiconductors	Nijmegen
D. Wind	Philips Semiconductors	Nijmegen
J. Knol	Philips Semiconductors	Nijmegen
H. Elzinga	Philips Semiconductors	Nijmegen
M. Stoutjesdijk	Philips Semiconductors	Nijmegen
T. Brand	Philips Semiconductors	Nijmegen
H. Gellersen	Philips Semiconductors	Hamburg
M. Schlüter	Philips Semiconductors	Hamburg
R. Velghe	Philips Semiconductors	Crolles
A. Yao	Philips Semiconductors	Sunnyvale
S. Harker	Philips Semiconductors	Albuquerque

©Philips Electronics N.V. 1998

S. Bardy	Philips Composants	Caen
S. Hausser	SMST	Boeblingen
U. Kehrli	FASELEC	Zürich
J. Symons	ED&T Analogue Simulation	WAY-31
M. Vertregt	Philips Research	WAY-51
D. Wolters	Philips Research	WAG-11
A. Zegers	Philips Research	WAG-11
L. Tiemeijer	Philips Research	WAG-13
H. Tuinhout	Philips Research	WAG-11
P. Woerlee	Philips Research	WAG-1
W. Kloosterman	Philips Research	WAG-13
D. Klaassen	Philips Research	WAG-13
A. Scholten	Philips Research	WAG-1
C. Bastiaansen	Philips Research	WAY-51
J.C. Six	Philips Semiconductors	Caen
D. Meignant	Philips Semiconductors	Caen
D. Brunnel	Philips Semiconductors	Caen
P. Philippe	Philips Semiconductors	Caen
S.H. Lee	Philips Semiconductors	Sunnyvale
E. Wagner	Philips Semiconductors	Neurenberg
R. Becker	Philips Semiconductors	Zürich
S. Neukom	Philips Semiconductors	Zürich
R. Ryter	Philips Semiconductors	Zürich
M. Reber	Philips Semiconductors	Zürich
B. Robertson	Philips Semiconductors	Zürich

©Philips Electronics N.V. 1998